Computational Mechanics 14 (1994) 201–228 © Springer-Verlag 1994

Implementation of the transformation field analysis for inelastic composite materials

G. J. Dvorak, Y. A. Bahei-El-Din, A. M. Wafa

1 Introduction

The transformation field analysis is a new method for incremental solution of thermomechanical loading problems in inelastic heterogeneous media and composite materials, described in recent papers by Dvorak (1991, 1992). When used with a selected micromechanical model, the analysis provides piecewise uniform approximations of the instantaneous local strain and stress fields in the phases, and estimates of the overall instantaneous thermomechanical properties of a representative volume of the heterogeneous solid. The method incorporates many of the currently used approaches to problems of this kind as special cases, this is shown for the unit cell models, the Mori-Tanaka and the self-consistent methods, as well as for other methods that utilize the Eshelby solution. The purpose of the present paper is to examine several different aspects of numerical implementation of the method in solutions of problems for composite materials consisting of elastic-plastic, viscoelastic, and viscoplastic phases.

Starting with the assumption of an additive decomposition of the small total strains, the method regards all inelastic strains, or relaxation stresses, as eigenstrain or eigenstress fields, referred to jointly as transformation fields, in an otherwise elastic body. The residual fields generated by the transformation fields are evaluated with certain transformation influence functions, or concentration factor tensors. These follow from solutions of elastic problems for locally applied eigenstrains or eigenstresses, which can be constructed with several different micromechanical techniques, such as the self-consistent and Mori-Tanaka methods, or with unit cell models. Therefore, the influence functions depend only on the elastic moduli of the phases and on the geometry of the microstructure, and thus remain constant during deformation. Once determined, they are used to write a system of differential equations for evaluation of the local instantaneous strains or stresses. Many different constitutive relations can be easily introduced into the analysis. Moreover, if the influence functions are evaluated in accordance with the criteria outlined by Dvorak and Benveniste (1992), the results satisfy exact connections between certain volume averages of both the total strains or stresses, and the eigenstrains or eigenstresses.

The first three sections of the paper introduce some preliminary concepts: Sect. 2 contains a brief summary of various definitions of local and overall properties; Sect. 3 outlines the concept of eigenstress and eigenstrain influence functions and concentration factors, while Sect. 4 discusses in detail their evaluation in micromechanical unit cell models by the finite element method. The essence of the transformation field analysis method is described in Sect. 5. This is followed by examples of applications to composites with elastic-plastic, viscoelastic, and viscoplastic phases.

The notation used is fashioned after that introduced by Hill (1963); (6×1) vectors are denoted by boldface lower case Roman or Greek letters, (6×6) matrices by boldface uppercase Roman letters, and $\mathbf{A}\mathbf{A}^{-1} = \mathbf{A}^{-1}\mathbf{A} = \mathbf{I}$, if the inverse exists. Scalars are denoted by lightface letters. Scripts characters are reserved for quantities that change during deformation. Volume averages of fields in V_r, such as $\mathbf{A}_r(\mathbf{x})$ or $\boldsymbol{\varepsilon}_r(\mathbf{x})$, or of $\boldsymbol{\sigma}(\mathbf{x})$ in V are denoted by $\mathbf{A}_r$, $\boldsymbol{\varepsilon}_r$ or $\boldsymbol{\sigma}$.

2 Local and overall properties

We consider a certain representative volume V of a heterogeneous solid, such as a composite or polycrystal, made of many perfectly bonded phases $r = 1, 2, \ldots N$, residing in volumes $V_r \in V$. The response of the

Communicated by S. N. Atluri, 4 September 1993

G. J. Dvorak, A. M. Wafa
Center for Composite Materials and Structures, Rensselaer Polytechnic Institute, Troy, NY 12180, USA

Y. A. Bahei-El-Din
Structural Engineering Department, Cairo University, Giza, Egypt

This work was supported by the Air Force Office of Scientific Research, and by the Office of Naval Research

phases may be represented by various inviscid or time-dependent constitutive relations to be discussed below, providing that at any time t the total strains and stresses can be additively decomposed as

$$\boldsymbol{\varepsilon}_r(\mathbf{x}, t) = \boldsymbol{\varepsilon}_r^e(\mathbf{x}, t) + \boldsymbol{\mu}_r(\mathbf{x}, t) \qquad \boldsymbol{\sigma}_r(\mathbf{x}, t) = \boldsymbol{\sigma}_r^e(\mathbf{x}, t) + \boldsymbol{\lambda}_r(\mathbf{x}, t), \tag{1}$$

where x denotes the material coordinates in a selected cartesian system associated with V. The $\boldsymbol{\varepsilon}_r^e$ and $\boldsymbol{\mu}_r$ in (1_1) denote, respectively, the elastic strain due to certain surface tractions at the boundary of V_r, and an eignstrain in the phase r. Similarly, the $\boldsymbol{\sigma}_r^e$ and $\boldsymbol{\lambda}_r$ in (1_2) denote the elastic stress and eigenstress in phase r under certain surface displacements applied at the surface of V_r.

The eigenstrain and eigenstress fields, henceforth referred to jointly as transformation fields, may consist of contributions of distinct physical origin, and thus may be decomposed further. For example, if only thermal and inelastic effects are considered,

$$\boldsymbol{\mu}_r(\mathbf{x}, t) = \mathbf{m}_r\theta(t) + \boldsymbol{\varepsilon}_r^{\text{in}}(\mathbf{x}, t) + \cdots \qquad \boldsymbol{\lambda}_r(\mathbf{x}, t) = \mathbf{l}_r\theta(t) + \boldsymbol{\sigma}_r^{\text{re}}(\mathbf{x}, t) + \cdots, \tag{2}$$

where $\mathbf{m}_r$ and $\mathbf{l}_r$ are the thermal strain and stress tensors. The coefficients of $\mathbf{m}_r$ represent the linear thermal expansion coefficients, the $\boldsymbol{\varepsilon}_r^{\text{in}}$ denotes an inelastic strain, and $\boldsymbol{\sigma}_r^{\text{re}}$ a relaxation stress. Contributions due to the other transformation effects can be added.

With these definitions, (1) become

$$\begin{aligned} \boldsymbol{\varepsilon}_r(\mathbf{x}, t) &= \mathbf{M}_r\boldsymbol{\sigma}_r(\mathbf{x}, t) + \mathbf{m}_r\theta(t) + \boldsymbol{\varepsilon}_r^{\text{in}}(\mathbf{x}, t) \\ \boldsymbol{\sigma}_r(\mathbf{x}, t) &= \mathbf{L}_r\boldsymbol{\varepsilon}_r(\mathbf{x}, t) + \mathbf{l}_r\theta(t) + \boldsymbol{\sigma}_r^{\text{re}}(\mathbf{x}, t), \end{aligned} \tag{3}$$

together with the interrelations

$$\mathbf{m}_r = -\mathbf{M}_r\mathbf{l}_r \qquad \boldsymbol{\varepsilon}_r^{\text{in}}(\mathbf{x}, t) = -\mathbf{M}_r\boldsymbol{\sigma}_r^{\text{re}}(\mathbf{x}, t)$$

$$\mathbf{l}_r = -\mathbf{L}_r\mathbf{m}_r \qquad \boldsymbol{\sigma}_r^{\text{re}}(\mathbf{x}, t) = -\mathbf{L}_r\boldsymbol{\varepsilon}_r^{\text{in}}(\mathbf{x}, t), \tag{4}$$

where $\mathbf{L}_r$ and $\mathbf{M}_r = \mathbf{L}_r^{-1}$ are the elastic phase stiffness and compliance tensors, assumed to be diagonally symmetric, positive definite, and for now, independent of temperature.

In describing the overall response of the heterogeneous medium, we focus on a representative volume V, defined either as a sufficiently large sample that contains many phases and reflects typical macroscopic properties (Hill 1963), or as a suitably selected unit cell of a (usually) periodic model of the actual material geometry. In either case, macroscopically homogeneous response and the implied existence of certain overall or effective properties are assumed under macroscopically uniform overall stress $\boldsymbol{\sigma}(t)$ or uniform overall strain $\boldsymbol{\varepsilon}(t)$, prescribed through surface tractions or displacements specified on the surface S of V. In unit cell models, the uniform overall quantities must be reduced to certain periodic boundary conditions for the representative cell.

With these definitions, the overall and local fields are connected by

$$\boldsymbol{\varepsilon}(t) = \frac{1}{V}\int_V \boldsymbol{\varepsilon}_r(\mathbf{x}, t)\, dV \qquad \boldsymbol{\sigma}(t) = \frac{1}{V}\int_V \boldsymbol{\sigma}_r(\mathbf{x}, t)\, dV. \tag{5}$$

When phase eigenstrains are present, the above definition of the representative volume needs to be expanded to incorporate overall response of the heterogeneous solid to local eigenstrains in phases or subvolumes of such phases. In particular, let $\boldsymbol{\mu}(\mathbf{x}, t)$ denote an eigenstrain field defined in V such that, if the surface S of V is traction-free, this field causes surface displacements on S that are consistent with a macroscopically uniform overall strain $\boldsymbol{\mu}(t)$. Similarly, if the volume V is constrained such that no displacements are permitted on the surface S, then, $\boldsymbol{\lambda}(\mathbf{x}, t)$ denotes an eigenstress field defined in V such that it causes surface tractions on S that are consistent with a macroscopically uniform overall stress $\boldsymbol{\lambda}(t)$. In analogy with (2), the $\boldsymbol{\mu}(t)$ and $\boldsymbol{\lambda}(t)$ will be referred to as the overall transformation fields.

Recall now that the local and overall transformation fields are connected by the generalized Levin (1967) formula (Dvorak and Benveniste 1992, Eqs. 7 and 8)

$$\boldsymbol{\lambda}(t) = \frac{1}{V}\int_V \mathbf{A}_r^T(\mathbf{x})\,\boldsymbol{\lambda}_r(\mathbf{x}, t)\, dV \qquad \boldsymbol{\mu}(t) = \frac{1}{V}\int_V \mathbf{B}_r^T(\mathbf{x})\,\boldsymbol{\mu}_r(\mathbf{x}, t)\, dV, \tag{6}$$

where the $\mathbf{B}_r(\mathbf{x})$ and $\mathbf{A}_r(\mathbf{x})$ are the mechanical stress and strain influence functions. If the transformation fields in (2) are caused only by a uniform change in temperature, then the mechanical and thermal

influence functions define the local fields as

$$\boldsymbol{\sigma}_r(\mathbf{x}, t) = \mathbf{B}_r(\mathbf{x})\,\boldsymbol{\sigma}(t) + \mathbf{b}_r(\mathbf{x})\,\theta(t) \qquad \boldsymbol{\varepsilon}_r(\mathbf{x}, t) = \mathbf{A}_r(\mathbf{x})\,\boldsymbol{\varepsilon}(t) + \mathbf{a}_r(\mathbf{x})\,\theta(t), \tag{7}$$

where the $\mathbf{b}_r(\mathbf{x})$ and $\mathbf{a}_r(\mathbf{x})$ are the thermoelastic influence functions.

In actual solutions, the continuous fields are usually replaced by piecewise uniform approximations in the phases or in subvolumes Ω_ρ, $\rho = 1, 2, \ldots M$, of a discretized unit cell. Then, (5) and (6) are reduced to

$$\boldsymbol{\varepsilon}(t) = \sum_{\rho=1}^{M} c_\rho\,\boldsymbol{\varepsilon}_\rho(t) \qquad \boldsymbol{\sigma}(t) = \sum_{\rho=1}^{M} c_\rho\,\boldsymbol{\sigma}_\rho(t) \tag{8}$$

$$\boldsymbol{\lambda}(t) = \sum_{\rho=1}^{M} c_\rho\,\mathbf{A}_\rho^T\boldsymbol{\lambda}_\rho(t) \qquad \boldsymbol{\mu}(t) = \sum_{\rho=1}^{M} c_\rho\,\mathbf{B}_\rho^T\boldsymbol{\mu}_\rho(t), \tag{9}$$

where the concentration factor tensors $\mathbf{B}_\rho$ and $\mathbf{A}_\rho$ represent the volume averages of the respective influence functions over Ω_ρ.

With regard to (5) and (6), or (8) and (9), the relation between the overall total and transformation stresses and strains at any time t may be written in terms of the overall elastic stiffness $\mathbf{L}$, and compliance $\mathbf{M}$,

$$\boldsymbol{\varepsilon}(t) = \mathbf{M}\,\boldsymbol{\sigma}(t) + \boldsymbol{\mu}(t) \qquad \boldsymbol{\sigma}(t) = \mathbf{L}\,\boldsymbol{\varepsilon}(t) + \boldsymbol{\lambda}(t), \tag{10}$$

where $\mathbf{M} = \mathbf{L}^{-1}$, $\boldsymbol{\lambda}(t) = -\mathbf{L}\,\boldsymbol{\mu}(t)$, $\boldsymbol{\mu}(t) = -\mathbf{M}\,\boldsymbol{\lambda}(t)$.

If the decomposition (2) is applied to the overall quantities, one recovers

$$\boldsymbol{\varepsilon}(t) = \mathbf{M}\,\boldsymbol{\sigma}(t) + \mathbf{m}\,\theta(t) + \boldsymbol{\varepsilon}^{in}(t) \qquad \boldsymbol{\sigma}(t) = \mathbf{L}\,\boldsymbol{\varepsilon}(t) + \mathbf{l}\,\theta(t) + \boldsymbol{\sigma}^{re}(t), \tag{11}$$

and the relations (6) and (7) provide the well-known connections (Hill 1963; Laws 1973)

$$\mathbf{L} = \sum_{\rho=1}^{M} c_\rho\,\mathbf{L}_\rho\mathbf{A}_\rho \qquad \mathbf{M} = \sum_{\rho=1}^{M} c_\rho\,\mathbf{M}_\rho\mathbf{B}_\rho \tag{12}$$

$$\mathbf{l} = \sum_{\rho=1}^{M} c_\rho(\mathbf{l}_\rho + \mathbf{L}_\rho\mathbf{a}_\rho) \qquad \mathbf{m} = \sum_{\rho=1}^{M} c_\rho(\mathbf{m}_\rho + \mathbf{M}_\rho\mathbf{b}_\rho), \tag{13}$$

where $\mathbf{L}$ and $\mathbf{M} = \mathbf{L}^{-1}$ are the overall elastic stiffness and compliance tensors, and $\mathbf{l}$, $\mathbf{m} = -\mathbf{M}\mathbf{l}$ are the overall thermal stress and strain tensors.

3
Local fields

Under purely thermoelastic deformation of the heterogeneous aggregate, the local fields are provided by (7), as a superposition of the contributions due to the overall mechanical stresses and strains, and the thermally induced local transformations in (2). In the same spirit, one can superimpose the effect of any other local transformation field $\boldsymbol{\mu}(\mathbf{x}, t)$, or $\boldsymbol{\lambda}(\mathbf{x}, t)$ by writing the local fields in the form (Dvorak 1990)

$$\boldsymbol{\varepsilon}_r(\mathbf{x}, t) = \mathbf{A}_r(\mathbf{x})\,\boldsymbol{\varepsilon}(t) + \mathbf{D}_r(\mathbf{x}, \mathbf{x}')\,\boldsymbol{\mu}(\mathbf{x}', t), \qquad \boldsymbol{\sigma}_r(\mathbf{x}, t) = \mathbf{B}_r(\mathbf{x})\,\boldsymbol{\sigma}(t) + \mathbf{F}_r(\mathbf{x}, \mathbf{x}')\,\boldsymbol{\lambda}(\mathbf{x}', t). \tag{14}$$

Noting that (2) to (4) imply

$$\boldsymbol{\mu}(\mathbf{x}', t) = -\mathbf{M}(\mathbf{x}')\,\boldsymbol{\lambda}(\mathbf{x}', t) \qquad \boldsymbol{\lambda}(\mathbf{x}', t) = -\mathbf{L}(\mathbf{x}')\,\boldsymbol{\mu}(\mathbf{x}', t), \tag{15}$$

we observe that $\mathbf{F}_r(\mathbf{x}, \mathbf{x}')$ and $\mathbf{D}_r(\mathbf{x}, \mathbf{x}')$ are eigenstress and eigenstrain influence functions which evaluate the effect at $\mathbf{x}$ induced by a transformation at $\mathbf{x}'$ under overall uniform applied stress $\boldsymbol{\sigma}(t)$ or strain $\boldsymbol{\varepsilon}(t)$. For a stress-free homogeneous medium with a transformed ellipsoidal inclusion, $\mathbf{D}(\mathbf{x}', \mathbf{x}') = \mathbf{S}$, the Eshelby tensor.

The transformation influence functions can be easily connected to the integral equations formulation of the problem. Indeed, Dvorak and Benveniste (1992) show that

$$\mathbf{D}(\mathbf{x}, \mathbf{x}')\,\boldsymbol{\mu}(\mathbf{x}') = -\int_V \boldsymbol{\Gamma}(\mathbf{x}, \mathbf{x}')\,[(\mathbf{L}(\mathbf{x}') - \mathbf{L}^0)\,\mathbf{D}(\mathbf{x}, \mathbf{x}') - \mathbf{L}(\mathbf{x}')]\,\boldsymbol{\mu}(\mathbf{x}')\,d\mathbf{x}', \tag{16}$$

where $\mathbf{L}^0$ is the stiffness of a comparison homogeneous medium, and

$$\Gamma_{ijkl}(\mathbf{x},\mathbf{x}') = -\frac{1}{2}(G_{ik,jl}(\mathbf{x},\mathbf{x}') + G_{jk,il}(\mathbf{x},\mathbf{x}')), \tag{17}$$

where G_{ik} is the Green's function of the medium $\mathbf{L}^0$ that satisfies

$$\mathbf{L}^0_{ijkl}\mathbf{G}_{kp,lj}(\mathbf{x},\mathbf{x}') + \delta_{ip}\delta(\mathbf{x}-\mathbf{x}') = 0, \quad \mathbf{x},\mathbf{x}'\in V, \tag{18}$$

where δ_{ip} is the Kronecker symbol, and $\delta(\mathbf{x}-\mathbf{x}')$ is the Dirac delta function.

In actual evaluations of the local elastic and transformation fields, the respective influence functions in (14), and all components of the local fields, are sought in terms of averages, and piecewise uniform approximations, respectively, within phase volumes V_r, or subvolumes or subelements Ω_ρ of discretized phases. In particular, the representative volume V, or the unit cell volume Ω, are subdivided into subelements $\rho, \eta = 1, 2, \ldots M$ of volume $\Omega_\rho, \Omega_\eta \in V_r$, where $M \geqq N$, so that each subelement resides in only one phase r. Conversely, each phase may contain one or more subelements. The stresses and strains are approximated as uniform in each Ω_ρ, Ω_η, and, if all local transformations (2) are superimposed, (14) is replaced by

$$\boldsymbol{\varepsilon}_\rho(t) = \mathbf{A}_\rho\boldsymbol{\varepsilon}(t) + \sum_{\eta=1}^{M}\mathbf{D}_{\rho\eta}[\mathbf{m}_\eta\theta(t) + \boldsymbol{\varepsilon}^{\mathrm{in}}_\eta(t)] \tag{19}$$

$$\boldsymbol{\sigma}_\rho(t) = \mathbf{B}_\rho\boldsymbol{\sigma}(t) + \sum_{\eta=1}^{M}\mathbf{F}_{\rho\eta}[\mathbf{l}_\eta\theta(t) + \boldsymbol{\sigma}^{\mathrm{re}}_\eta(t)]. \tag{20}$$

This form describes the response of the elastic composite to certain uniform overall mechanical fields and piecewise uniform local transformation fields. The $\mathbf{A}_\rho$ and $\mathbf{B}_\rho$ are the mechanical concentration factor tensors. Under overall strain $\boldsymbol{\varepsilon}(t) = \mathbf{0}$, the $\mathbf{D}_{\rho\eta}$ gives the strain caused in Ω_ρ by a unit uniform eigenstrain located in Ω_η. Under overall stress $\boldsymbol{\sigma}(t) = \mathbf{0}$, the $\mathbf{F}_{\rho\eta}$ defines the stress in Ω_ρ due to a unit eigenstress in Ω_η. Any additional eigenstrains or eigenstresses of interest can be incorporated. In what follows, the $\mathbf{D}_{\rho\eta}$ and $\mathbf{F}_{\rho\eta}$ will be referred to as the transformation concentration factor tensors.

Before proceeding to some simple examples of these tensors, we note that their evaluation by the finite element method, which is of interest in unit cell models, is outlined in Sect. 4 below. A particularly simple evaluation is possible in two-phase media, with phases denoted as $r = \alpha, \beta$. According to Dvorak (1990, Eqs. 123–125)

$$\mathbf{D}_{r\alpha} = (\mathbf{I}-\mathbf{A}_r)(\mathbf{L}_\alpha-\mathbf{L}_\beta)^{-1}\mathbf{L}_\alpha \qquad \mathbf{D}_{r\beta} = -(\mathbf{I}-\mathbf{A}_r)(\mathbf{L}_\alpha-\mathbf{L}_\beta)^{-1}\mathbf{L}_\beta \tag{21}$$

$$\mathbf{F}_{r\alpha} = (\mathbf{I}-\mathbf{B}_r)(\mathbf{M}_\alpha-\mathbf{M}_\beta)^{-1}\mathbf{M}_\alpha \qquad \mathbf{F}_{r\beta} = -(\mathbf{I}-\mathbf{B}_r)(\mathbf{M}_\alpha-\mathbf{M}_\beta)^{-1}\mathbf{M}_\beta. \tag{22}$$

In multiphase media, the expressions for the concentration factor tensors were found by Dvorak and Benveniste (1992) in terms of estimates derived with the self-consistent or Mori-Tanaka methods. For both methods, the results are

$$\mathbf{D}_{rs} = (\mathbf{I}-\mathbf{A}_r)(\mathbf{L}_r-\mathbf{L})^{-1}(\delta_{rs}\mathbf{I}-c_s\mathbf{A}_s^T)\mathbf{L}_s \tag{23}$$

$$\mathbf{F}_{rs} = (\mathbf{I}-\mathbf{B}_r)(\mathbf{M}_r-\mathbf{M})^{-1}(\delta_{rs}\mathbf{I}-c_s\mathbf{B}_s^T)\mathbf{M}_s, \qquad r,s = 1,2\ldots N \tag{24}$$

where the $\mathbf{L}$ and $\mathbf{M}$ are the respective estimates of the overall elastic stiffness and compliance tensors, while $\mathbf{A}_r$ and $\mathbf{B}_r$ are the related estimates of the elastic mechanical concentration factor tensors; $\mathbf{L}_r$, $\mathbf{M}_r$ are the phase elastic properties. The δ_{rs} is the Kronecker symbol, but no summation is indicated by repeated indices. It can be verified that in two-phase media, (23) and (24) reduce to (21) and (22).

It should be noted that applications of the self-consistent and Mori-Tanaka methods to specific material systems are restricted by certain admissibility conditions which, in the present example, are satisfied by any two-phase materials and by those multiphase solids that contain or consist of inclusions of similar shape and alignment (Dvorak and Benveniste 1992).

If the overall eigenstrain $\boldsymbol{\mu}(t)$ in (9_2) is used in (10_1), and the resulting total strain $\boldsymbol{\varepsilon}(t)$ is then substituted into (19), where the $\boldsymbol{\varepsilon}_\rho(t)$ is written in terms of the local stresses in (2_1), (3_2), one finds

$$\boldsymbol{\sigma}_\rho(t) = \mathbf{L}_\rho\mathbf{A}_\rho\mathbf{M}\,\boldsymbol{\sigma}(t) - \mathbf{L}_\rho\sum_{\eta=1}^{M}[(c_\eta\mathbf{A}_\rho\mathbf{B}_\eta^T + \mathbf{D}_{\rho\eta})\mathbf{M}_\eta\lambda_\eta(t)] + \boldsymbol{\lambda}_\rho(t). \tag{25}$$

When compared with (20), this provides the connections

$$\mathbf{A}_\rho \mathbf{M} = \mathbf{M}_\rho \mathbf{B}_\rho \qquad \mathbf{F}_{\rho\eta} = \mathbf{L}_\rho [\delta_{\rho\eta}\mathbf{I} - c_\eta \mathbf{A}_\rho \mathbf{B}_\eta^T - \mathbf{D}_{\rho\eta}]\mathbf{M}_\eta$$

$$\sum_{\rho=1}^{M} c_\rho \mathbf{A}_\rho = \mathbf{I} \qquad \sum_{\rho=1}^{M} c_\rho \mathbf{B}_\rho = \mathbf{I}. \tag{26}$$

Moreover, using (4), (7) and (19), (20) one finds that

$$\mathbf{a}_\rho = \sum_{\eta=1}^{M} \mathbf{D}_{\rho\eta}\mathbf{m}_\eta = -\sum_{\eta=1}^{M} \mathbf{D}_{\rho\eta}\mathbf{M}_\eta \mathbf{l}_\eta, \qquad \mathbf{b}_\rho = \sum_{\eta=1}^{M} \mathbf{F}_{\rho\eta}\mathbf{l}_\eta = -\sum_{\eta=1}^{M} \mathbf{F}_{\rho\eta}\mathbf{L}_\eta \mathbf{m}_\eta. \tag{27}$$

4
Influence functions for unit cell models

4.1
Procedure

The results (21) to (24) provide simple estimates of the transformation concentration factor tensors of individual phases, but their accuracy may prove inadequate when the transformation fields exhibit large variations, as they do for example, during inelastic deformation. Subdivision of the phases is then indicated, and is usually accomplished in the context of a unit cell model of an idealized composite material. If a periodic arrangement of the microstructure is selected, then the unit cell is subjected to appropriate periodic boundary conditions, and the local fields are evaluated by the finite element method. Many such models have been described in the literature; in the examples that follow, we will utilize the periodic hexagonal array (PHA) model of a fibrous composite (Dvorak and Teply 1985; Teply and Dvorak 1988).

To illustrate the finite element evaluation of the piecewise uniform approximations (19) and (20) of the influence functions in (14), we subdivide the domain under consideration by constant strain 3D elements Ω_η, $\eta = 1, 2, \ldots M$, interconnected at nodes $i, j, \ldots = 1, 2, \ldots R$. The coefficients of the mechanical strain or stress concentration factor tensors $\mathbf{A}_\eta$ or $\mathbf{B}_\eta$ in (19) or (20) are then found from solutions of six successive elasticity problems. In each solution, the domain, free from any eigenstrains, is subjected to overall strain $\boldsymbol{\varepsilon}$, or stress $\boldsymbol{\sigma}$, that have only one nonzero component of unit magnitude. The (6 × 1) strain or stress vector found in the element Ω_η is the column of the (6 × 6) matrix $\mathbf{A}_\eta$ or $\mathbf{B}_\eta$, corresponding to the selected nonzero component.

The transformation concentration factors can be obtained in a similar way, by applying, in turn, each single component of a unit eigenstrain vector $\boldsymbol{\mu}_\rho$ in the element Ω_ρ within an otherwise strain-free domain, and finding the local strains in all elements. Each such local strain in Ω_η represents one column of the (6 × 6) matrix $\mathbf{D}_{\eta\rho}$ for Ω_η in (19). An analogous sequence involving substitution of the $\mathbf{D}_{\eta\rho}$ matrices in (26$_2$), yields the columns of $\mathbf{F}_{\eta\rho}$. If the evaluation of the $\mathbf{D}_{\eta\rho}$ and $\mathbf{F}_{\eta\rho}$ matrices is made using a standard finite element code, the unit local eigenstrains may be produced as thermal strains, by appropriate selections of nonzero thermal expansion coefficients.

A much more efficient evaluation of these matrices is possible using the stiffness matrix of the unit cell domain. In each constant strain element, the displacement $\mathbf{u}$ at any point within the element Ω_η is approximated by

$$\mathbf{u}_\eta = \mathbf{N}_\eta \boldsymbol{\alpha}_\eta \tag{28}$$

where $\mathbf{N}_\eta = [\mathbf{N}_i^\eta \mathbf{N}_j^\eta \ldots]$ represents prescribed functions of position, and $\boldsymbol{\alpha}_\eta = [\boldsymbol{\alpha}_i^\eta \boldsymbol{\alpha}_j^\eta \ldots]^T$ is a listing of nodal displacements for a particular element. The strains at any point within Ω_η can be found as (the * is used to distinguish FEM terms from similarly denoted but different micromechanical terms).

$$\boldsymbol{\varepsilon}_\eta = \overset{*}{\mathbf{S}}\mathbf{u}_\eta = \overset{*}{\mathbf{S}}\mathbf{N}_\eta \boldsymbol{\alpha}_\eta = \overset{*}{\mathbf{B}}_\eta \boldsymbol{\alpha}_\eta \qquad \overset{*}{\mathbf{B}}_\eta = [\overset{*}{\mathbf{B}}_i^\eta \overset{*}{\mathbf{B}}_j^\eta \ldots] = \overset{*}{\mathbf{S}}\mathbf{N}_\eta, \tag{29}$$

where $\overset{*}{\mathbf{S}}$ is a suitable linear differential operator. Since the element strain field is required to be uniform, the shape functions, $\mathbf{N}_i^\eta, \mathbf{N}_j^\eta, \ldots$, etc., must be linear in the coordinates $\mathbf{x}_1, \mathbf{x}_2, \mathbf{x}_3$, and the coefficient matrix $\overset{*}{\mathbf{B}}_\eta$ in (29) is constant.

With reference to (3), (4), the relationship between stress and strain in the element Ω_η that contains a uniform eigenstrain $\boldsymbol{\mu}_\eta$ is

$$\boldsymbol{\sigma}_\eta = \mathbf{L}_\eta(\boldsymbol{\varepsilon}_\eta - \boldsymbol{\mu}_\eta). \tag{30}$$

The stress $\boldsymbol{\sigma}_\eta$ in the element and the tractions on the element surface can be reproduced by subjecting the element to the nodal force $\mathbf{q}_\eta = [\mathbf{q}_i^\eta \mathbf{q}_j^\eta \ldots]^T$, statically equivalent to the element stresses and boundary tractions, found from the principle of virtual work. In the absence of body forces, the equivalent nodal force is given by the volume integral

$$\mathbf{q}_\eta = \int_{\Omega_\eta} \overset{*}{\mathbf{B}}{}_\eta^T \boldsymbol{\sigma}_\eta \, d\Omega_\eta. \tag{31}$$

Since only constant stress and strain fields are admitted in the elements, the $\overset{*}{\mathbf{B}}_\eta$ is constant, and the integral in (31) can be evaluated in closed form. Substituting the constitutive Eq. (30) into (31), and using the strain-displacement relation given in (29), we can write the equivalent nodal forces associated with node i of element Ω_η as

$$\mathbf{q}_i^\eta = \sum_{j=1}^{P} \mathbf{K}_{ij}^\eta \boldsymbol{\alpha}_j^\eta + \mathbf{f}_i^\eta \tag{32}$$

$$\mathbf{K}_{ij}^\eta = \overset{*}{\mathbf{B}}{}_i^{\eta T} \mathbf{L}_\eta \overset{*}{\mathbf{B}}{}_j^\eta \Omega_\eta \tag{33}$$

$$\mathbf{f}_i^\eta = -\overset{*}{\mathbf{B}}{}_i^{\eta T} \mathbf{L}_\eta \boldsymbol{\mu}_\eta \Omega_\eta, \tag{34}$$

where P is the total number of element nodes, $\mathbf{K}_{ij}^\eta$ is the ij partition of the element stiffness matrix, and $\mathbf{f}_i^\eta$ represents the forces at node i caused by the uniform eigenstrains $\boldsymbol{\mu}_\eta$.

When the solution domain Ω is not subjected to any external loads, the sum of the forces at a generic node i contributed by the elements connected to that node must vanish. Therefore, at each such node

$$\sum_{\eta=1}^{M} \mathbf{q}_i^\eta = 0 \qquad i = 1, 2, \ldots R, \tag{35}$$

where M is the total number of elements, and R is the total number of nodes in the domain. Substituting (32) into (35), one finds

$$\sum_{\eta=1}^{M} \sum_{j=1}^{P} \mathbf{K}_{ij}^\eta \boldsymbol{\alpha}_j^\eta = -\sum_{\eta=1}^{M} \mathbf{f}_i^\eta \qquad i = 1, 2, \ldots R. \tag{36}$$

These R matrix equations can be augmented and written as

$$\mathbf{K}\boldsymbol{\alpha} = \mathbf{f} \tag{37}$$

$$\mathbf{K}_{ij} = \sum_{\eta=1}^{M} \mathbf{K}_{ij}^\eta \qquad \mathbf{f}_i = -\sum_{\eta=1}^{M} \mathbf{f}_i^\eta, \tag{38}$$

where $\mathbf{K}$ is the overall stiffness matrix, $\mathbf{f}$ is the overall load vector, and $\boldsymbol{\alpha} = [\boldsymbol{\alpha}_1 \boldsymbol{\alpha}_2 \ldots \boldsymbol{\alpha}_R]^T$ lists the as yet unknown nodal displacements.

The transformation factors $\mathbf{D}_{\rho\eta}$, $\rho, \eta = 1, 2, \ldots M$, can now be evaluated from the displacement field found by solving (37) and (38) for the $6M$ independent $\mathbf{f}$ vectors; each corresponds to an eigenstrain $\boldsymbol{\mu}_\eta = \mathbf{i}_k$, $k = 1, 2, \ldots 6$; $\eta = 1, 2, \ldots M$, where $\mathbf{i}_k$ is the k^{th} column of the (6×6) identity matrix. For example, if $k = 3$, then $\mathbf{i}_3 = [0\,0\,1\,0\,0\,0]^T$. In any case, the load vector $\mathbf{f}_i^\eta$ in (34) is

$$\mathbf{f}_i^\eta = -\overset{*}{\mathbf{B}}{}_i^{\eta T} \overset{*}{\mathbf{l}}{}_k^\eta \Omega_\eta \qquad \eta = 1, 2, \ldots M, \quad k = 1, 2, \ldots 6, \tag{39}$$

where $\overset{*}{\mathbf{l}}{}_k^\eta$ is the k^{th} column of the elastic stiffness matrix $\mathbf{L}_\eta$. According to (19), the overall strain must vanish when evaluating the strain transformation factors from the local strain field. Consequently, (37) must be subjected to displacement boundary conditions which are derived from a null overall strain vector.

Since the overall stiffness matrix $\mathbf{K}$ of the unit cell depends on the cell geometry, the finite element type and displacement shape functions and on material elastic properties, it is a constant matrix, and one may write (37) using (39) as

$$\mathbf{K}[\boldsymbol{\alpha}^{(1)} \boldsymbol{\alpha}^{(2)} \ldots \boldsymbol{\alpha}^{(6M)}]^T = [\mathbf{f}^{(1)} \mathbf{f}^{(2)} \ldots \mathbf{f}^{(6M)}]^T. \tag{40}$$

The matrix K can be evaluated for the unit cell domain Ω, and then decomposed to lower and upper triangular factors, $\mathbf{K}_L$ and $\mathbf{K}_U$, using Cholesky's method. Since K is symmetric, then $\mathbf{K}_U = \mathbf{K}_L^T$, and the nodal displacements $\boldsymbol{\alpha}^{(1)}, \boldsymbol{\alpha}^{(2)}, \ldots \boldsymbol{\alpha}^{(6M)}$ follow from forward and backward solutions of the following equations

$$\mathbf{K}_L [\mathbf{y}^{(1)} \mathbf{y}^{(2)} \ldots \mathbf{y}^{(6M)}]^T = [\mathbf{f}^{(1)} \mathbf{f}^{(2)} \ldots \mathbf{f}^{(6M)}]^T \tag{41}$$

$$\mathbf{K}_L^T [\boldsymbol{\alpha}^{(1)} \boldsymbol{\alpha}^{(2)} \ldots \boldsymbol{\alpha}^{(6M)}]^T = [\mathbf{y}^{(1)} \mathbf{y}^{(2)} \ldots \mathbf{y}^{(6M)}]^T. \tag{42}$$

Finally, the element nodal displacements $\boldsymbol{\alpha}_\eta$, $\eta = 1, 2, \ldots M$, are extracted from the solution for $\boldsymbol{\alpha}^{(i)}$, $i = 1, 2, \ldots 6M$, and substituted in (29_1) to obtain the strains $\boldsymbol{\varepsilon}_\eta$ which represent the columns of $\mathbf{D}_{\rho\eta}$; ρ, $\eta = 1, 2, \ldots M$. Let the matrix $\mathbf{P}_\rho$ relate the nodal displacements of element ρ to the overall displacement vector such that

$$\boldsymbol{\alpha}_\rho = \mathbf{P}_\rho \boldsymbol{\alpha}^{(i)} \qquad \rho = 1, 2, \ldots M,\ i = 1, 2, \ldots 6M. \tag{43}$$

From (29), we find

$$\boldsymbol{\varepsilon}_\rho = \overset{*}{\mathbf{B}}_\rho \mathbf{P}_\rho \boldsymbol{\alpha}^{(i)} = \tilde{\mathbf{P}}_\rho \boldsymbol{\alpha}^{(i)} \qquad \tilde{\mathbf{P}}_\rho = \overset{*}{\mathbf{B}}_\rho \mathbf{P}_\rho. \tag{44}$$

For a specific vector f in (37) which corresponds to unit eigenstrain $\boldsymbol{\mu}_\eta = \mathbf{i}_k$, $k = 1, 2, \ldots 6$, as given by (39), the strain in (44) represents the k^{th} column $\mathbf{d}_{\rho\eta}^k$ of the factor $\mathbf{D}_{\rho\eta}$. This can be written symbolically as

$$\mathbf{d}_{\rho\eta}^k = \tilde{\mathbf{P}}_\rho \mathbf{K}^{-1} \mathbf{f}. \tag{45}$$

An efficient way of obtaining $\mathbf{d}_{\rho\eta}^k$ is indicated by (41), (42) and (44).

The stress transformation factors $\mathbf{F}_{\rho\eta}$ follow from (26_2). Alternately, one can retrace the procedure leading to (41) and (42), but for f vectors corresponding to 6M unit eigenstress vectors $\lambda_\eta = \mathbf{i}_k$, $k = 1, 2, \ldots 6$. Since $\boldsymbol{\mu}_\eta = -\mathbf{M}_\eta \lambda_\eta$, (34) provides

$$\mathbf{f}_i^\eta = \overset{*}{\mathbf{b}}_{ik}^\eta \Omega_\eta \qquad \eta = 1, 2, \ldots M,\ k = 1, 2, \ldots 6, \tag{46}$$

where $\overset{*}{\mathbf{b}}_{ik}^\eta$ is the k^{th} column of matrix $\overset{*}{\mathbf{B}}_i^{\eta T}$. According to (20), the overall stress must vanish when evaluating the stress transformation factors from the local stress field. In this case, the solution of (41), (42), (44), together with (46) and (1_2), can be used to find the factors $\mathbf{F}_{\rho\eta}$. Symbolically, the k^{th} column $\overset{*}{\mathbf{f}}_{\rho\eta}^k$ of the $\mathbf{F}_{\rho\eta}$ factor corresponding to $\lambda_\eta = \mathbf{i}_k$ can be written as

$$\overset{*}{\mathbf{f}}_{\rho\eta}^k = \mathbf{L}_\rho \tilde{\mathbf{P}}_\rho \mathbf{K}^{-1} \mathbf{f} + \delta_{\rho\eta} \mathbf{i}_k, \tag{47}$$

where $\delta_{\rho\eta}$ is the Kronecker symbol, and f is assembled from the load vectors in (46) using (38_2).

4.2 Efficiency and accuracy

To asses the time required for evaluation of the transformation concentration factor $\mathbf{D}_{\rho\eta}$, we recall that the time needed for decomposition of the stiffness matrix K is proportional to the number of multiplications $\frac{1}{2} eRb^2$ involved in the Cholesky decomposition procedure, where e is the number of degrees of freedom at a node ($e = 3$ for 3D solid elements), and b is the half band width of K. The number of multiplications, required to evaluate the overall stiffness matrix for transversely isotropic elastic symmetry from (33) and (38), truns out to be 2388 M. The computation time required for solving (41) or (42) for each $\mathbf{f}^{(s)}$ vector, $s = 1, \ldots 6M$, is proportional to eRb. Hence, the total time for evaluation of the nodal displacements from (40) is proportional to $\{eRb(\frac{1}{2}b + 6M) + 2388\,\text{M}\}$. In some applications, where only certain (matrix) elements are allowed to develop inelastic strains, it is sufficient to find the eigenstrain concentration factors only for the potentially inelastic elements. If their number is T, $T \leqq M$, the time required for solving (40) is reduced to $\{eRb(\frac{1}{2}b + 6T) + 2388\,\text{M}\}$.

For each nodal displacement vector $\boldsymbol{\alpha}^{(s)}$, $s = 1, \ldots 6T$, computed from (40), the strain transformation concentration factors are given by the elements strains defined in (29). This operation involves $6eP$ multiplications for each element and each $\boldsymbol{\alpha}^{(s)}$ vector; P is the number of element nodes. Hence, the total time required for evaluation of the eigenstrain concentration factors is proportional to 36 ePMT. The eigenstress concentration factors follow in a similar way, but an additional Eq. (30) is required for their evaluation. The number of multiplications in this case is 36 for each element and for each $\boldsymbol{\alpha}^{(s)}$, hence additional computer time proportional to 216 MT would be required.

To verify the accuracy of the numerical evaluation of the mechanical and transformation influence functions, one may compare the results with the general properties of these functions, derived by Dvorak and Benveniste (1992). We list the principal results here, and refer the reader to the above reference for specific proofs. There exist two exact relations for the actual transformation influence functions that evaluate the local fields in Ω_η caused by uniform transformations in Ω_ρ, c.f., (14), (19), and (20),

$$\sum_{\rho=1}^{M} \mathbf{D}_{\eta\rho}(\mathbf{x}) = \mathbf{I} - \mathbf{A}_\eta(\mathbf{x}) \qquad \sum_{\rho=1}^{M} \mathbf{F}_{\eta\rho}(\mathbf{x}) = \mathbf{I} - \mathbf{B}_\eta(\mathbf{x}) \tag{48}$$

$$\sum_{\rho=1}^{M} \mathbf{D}_{\eta\rho}(\mathbf{x}) M_\rho = 0 \qquad \sum_{\rho=1}^{M} \mathbf{F}_{\eta\rho}(\mathbf{x}) L_\rho = 0. \tag{49}$$

In addition, the concentration factor tensors in (19), (20) must satisfy

$$c_\eta \mathbf{D}_{\eta\rho}\mathbf{M}_\rho = c_\rho \mathbf{M}_\eta \mathbf{D}_{\rho\eta}^T \qquad c_\eta \mathbf{F}_{\eta\rho}\mathbf{L}_\rho = c_\rho \mathbf{L}_\eta \mathbf{F}_{\rho\eta}^T \tag{50}$$

$$\sum_{\rho=1}^{M} c_\rho \mathbf{D}_{\rho\eta} = \mathbf{0} \qquad \sum_{\rho=1}^{M} c_\rho \mathbf{F}_{\rho\eta} = \mathbf{0}, \tag{51}$$

where $\eta, \rho = 1, 2, \ldots M$, the number of elements, and $c_\eta = \Omega_\eta / V$. These connections are exact but not independent; note that (49) and (50) give (51). Actual solutions then show that only (48) and (49) or (51) are independent. This provides $(2 \times M)$ independent relations for the $(M \times M)$ unknown transformation concentration factor tensors.

4.3
Symmetric unit cells

Most unit cell models replace the actual materials geometry with a certain periodic approximation. Consequently, the unit cells themselves may posses internal symmetries that can facilitate evaluation of the transformation influence factors. While each sepcific unit cell geometry has to be considered separately, we illustrate the procedure that one may use for the periodic hexagonal array (PHA) model of fibrous composites that is described in greater detail in Sect. 6 below. A typical unit cell of the PHA model is a prism with an equilateral triangular cross section, Figs. 1–3, subjected to certain periodic boundary conditions described in detail by Teply and Dvorak (1988, Sect. 3).

The PHA model geometry has a 3-fold axis of rotational symmetry, parallel to the fiber axis that coincides with the cartesian coordinate direction x_1, and three planes of symmetry perpendicular to the transverse x_2x_3-plane. This provides for a subdivision of the solution domain into six similar triangular subdomains $A, B, \ldots F$, as shown in Fig. 1. The geometry of the finite element mesh in each of these subdomains is selected to be invariant under 120° rotations about the $x_1 \equiv x_1' \equiv x_1''$-axis, and under reflections about the x_2-axis, the x_2'-axis, and the x_2''-axis. Obviously, such selection does not rule out elements that cross the symmetry axes, c.f., Figs. 2, 3.

According to (19) and (20), the eigenstrain concentration factor $\mathbf{D}_{\rho\eta}$ is evaluated as the strain field ε_ρ in all subelements $\Omega_\rho \in \Omega$, $\rho = 1, 2, \ldots M$, caused by a unit eigenstrain $\boldsymbol{\mu}_\eta = \mathbf{i}_k$, $k = 1, 2, \ldots 6$, prescribed in any subelement $\Omega_\eta \in \Omega$, $\eta = 1, 2, \ldots M$, while the composite material is subjected to zero overall strain. The eigenstress concentration factors $\mathbf{F}_{\rho\eta}$ are found for similarly specified subelement eigenstresses in a composite subjected to zero overall tractions. These boundary conditions can be reproduced on the unit cell of the PHA model. Of course, the implication is that all unit cells comprising the fibrous composite material model experience identical unit eigenstrains or eigenstresses while the aggregate is subjected to zero overall strain or stress.

Under such circumstances, both the mesh and the boundary conditions remain invariant under the above described rotations and reflections, and it is then possible to show that the $\mathbf{D}_{\rho\eta}$ and $\mathbf{F}_{\rho\eta}$ matrices for element eigenstrains or eigenstresses prescribed within only one subdomain of the unit cell can be used to find the concentration factor matrices for eigenstrains or eigenstresses specified in any other subdomain.

While limiting attention to the $\mathbf{D}_{\rho\eta}$ matrices, where $\rho, \eta = 1, 2, \ldots M$ refers to all subelements M in Ω, we introduce the notation $\mathbf{D}_{\rho\alpha}$, $\mathbf{D}_{\rho\beta}$, $\mathbf{D}_{\rho\gamma}$, $\mathbf{D}_{\rho\delta}$, $\mathbf{D}_{\rho\varepsilon}$, $\mathbf{D}_{\rho\varphi}$ for subsets of the complete set of the $\mathbf{D}_{\rho\eta}$ matrices, found from unit eigenstrains introduced in the subdomains $A, B, \ldots F$ in Fig. 1. The one subset that needs to be constructed, e.g., with the procedure outlined in Sect. 4.1, is selected here as the $\mathbf{D}_{\rho\alpha}$, for unit eigenstrains $\boldsymbol{\mu}_\alpha = \mathbf{i}_k$, $\alpha = 1, 2, \ldots N$, $k = 1, 2, \ldots 6$, in the coordinate system x_j, $j = 1, 2, 3$; N denotes the number of subelements in the subdomain A. Each k^{th} column $\mathbf{d}_{\rho\alpha}^k$ of the matrix $\mathbf{D}_{\rho\alpha}$ represents the strain vector ε_ρ due to the single component $\boldsymbol{\mu}_\alpha = \mathbf{i}_k$ of the prescribed unit eigenstrain.

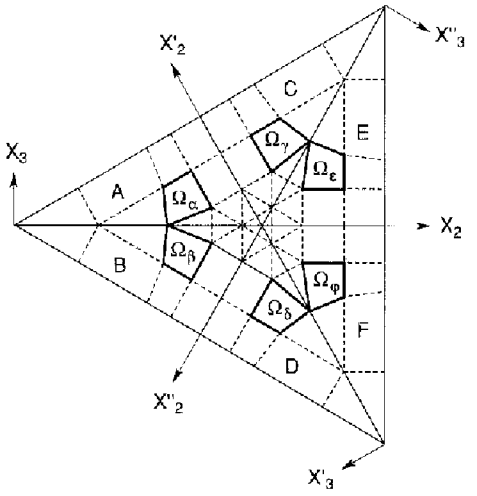

1

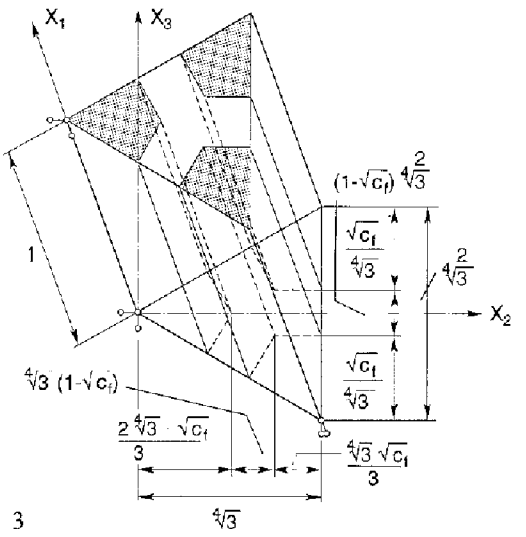

3

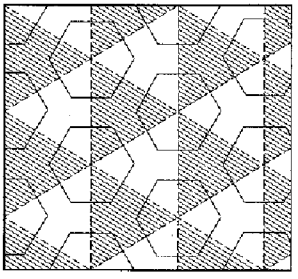

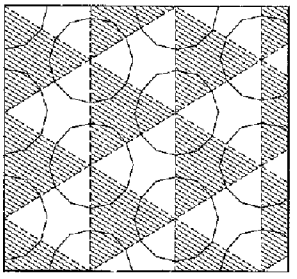

2

Figs. 1–3. 1 Subdomains of a unit cell. 2 Transverse cross sections of the PHA model microstructures with hexagonal and dodecagonal cylindrical fibers. 3 Geometry of the unit cell of the PHA model

Next, consider the subdomain D in the local coordinates x'_j, and locate the subelement volume $\Omega_\delta \in D$ that has the same position in the system x'_j as the volume $\Omega_\alpha \in A$ does in the coordinates x_j. In this subelement volume Ω_δ, introduce a uniform unit eigenstrain vector $\boldsymbol{\mu}_\delta = \mathbf{i}_k$, $k = 1, 2, \ldots 6$, defined in the x_j coordinates, to produce local strains $\mathbf{D}_{\rho\delta}\boldsymbol{\mu}_\delta$ in each of the subelements $\Omega_\rho \in \Omega$, $\rho = 1, 2, \ldots M$. Note that the applied unit eigenstrain $\boldsymbol{\mu}_\delta$ transforms into the eigenstrain $\boldsymbol{\mu}'_\delta$ in the x'_j-coordinates as

$$\boldsymbol{\mu}'_\delta = \boldsymbol{\Psi}\boldsymbol{\mu}_\delta = \boldsymbol{\Psi}\mathbf{i}_k = \boldsymbol{\psi}_k, \tag{52}$$

where $\boldsymbol{\Psi}$ is the transformation matrix, and $\boldsymbol{\psi}_k$ is its k^{th} column. For the 120° cw rotation implied in Fig. 1, and strain vectors defined as $[\varepsilon_{11}\, \varepsilon_{22}\, \varepsilon_{33}\, 2\varepsilon_{23}\, 2\varepsilon_{31}\, 2\varepsilon_{12}]^T$, $\boldsymbol{\Psi}$ is given by

$$\boldsymbol{\Psi} = \begin{bmatrix} 1 & 0 & 0 & 0 & 0 & 0 \\ 0 & 1/4 & 3/4 & -\sqrt{3}/4 & 0 & 0 \\ 0 & 3/4 & 1/4 & \sqrt{3}/4 & 0 & 0 \\ 0 & \sqrt{3}/2 & -\sqrt{3}/2 & -1/2 & 0 & 0 \\ 0 & 0 & 0 & 0 & -1/2 & -\sqrt{3}/2 \\ 0 & 0 & 0 & 0 & \sqrt{3}/2 & -1/2 \end{bmatrix}.$$

The existence of the three-fold rotational symmetry axis x_1 implies that local *unit* eigenstrains $\boldsymbol{\mu}_\alpha$ and $\boldsymbol{\mu}'_\delta$ introduced in volumes Ω_α and Ω_δ cause local strain fields in the respective x_j and x'_j coordinate systems that are invariant under the coordinate transformation from the x_j system to x'_j system. Therefore, the strain $\boldsymbol{\varepsilon}_\rho^{k\prime}$ described in the x'_j-coordinates in any selected volume Ω_ρ, caused by the eigenstrain (52), can be found with the help of (14_1) or (19) as

$$\boldsymbol{\varepsilon}_\rho^{k\prime} = \mathbf{D}_{\zeta z}\boldsymbol{\psi}_k, \tag{53}$$

where Ω_ζ is the subelement volume defined as that with the same position in the x_j coordinate system as the selected volume Ω_ρ does in the x'_j coordinate system. Then, the k^{th} column $\mathbf{d}_{\rho\delta}^k$ of the influence coefficient $\mathbf{D}_{\rho\delta}$, which relates the strain in volume Ω_ρ, $\rho = 1, 2, \ldots M$, to the unit eigenstrain

$\boldsymbol{\mu}_\delta$ prescribed in Ω_δ is given by the transformation of the strain vector (53) from the x_j' to the x_j coordinates. This can be written as

$$\mathbf{d}^k_{\rho\delta} = \boldsymbol{\Psi}^{-1}\mathbf{D}_{\zeta\alpha}\boldsymbol{\psi}_k \qquad k = 1, 2, \ldots 6, \tag{54}$$

and the transformation concentration factor matrix $\mathbf{D}_{\rho\delta}$ then follows from

$$\mathbf{D}_{\rho\delta} = \boldsymbol{\Psi}^{-1}\mathbf{D}_{\zeta\alpha}\boldsymbol{\Psi} \qquad \alpha, \delta = 1, 2, \ldots N; \quad \rho, \zeta = 1, 2, \ldots M. \tag{55}$$

As an example of the above procedure, we evaluate the matrix $\mathbf{D}_{\rho\delta}$, where Ω_ρ is any subelement volume in subdomain C, chosen to coincide with Ω_γ. First, we identify the volumes in the x_j-coordinates that correspond to the volumes Ω_γ and Ω_δ in the x_j'-coordinates; it is easy to see that they are the Ω_φ and Ω_α volumes, respectively. Therefore, (55) provides the matrix $\mathbf{D}_{\gamma\delta}$ as

$$\mathbf{D}_{\gamma\delta} = \boldsymbol{\Psi}^{-1}\mathbf{D}_{\varphi\alpha}\boldsymbol{\Psi}. \tag{56}$$

An analogous procedure can be applied to eigenstrains introduced in the subdomain E and associated with the x_j'' coordinate system. The relevant transformation is a 120°ccw rotation about x_1 into the x_j coordinate system.

To evaluate the subset $\mathbf{D}_{\rho\beta}$ for unit eigenstrains introduced in region B, one needs to utilize the x_1x_2-plane of symmetry in Fig. 1. In this case, the matrix $\boldsymbol{\Psi}$ in (52) is replaced by the matrix $\boldsymbol{\Psi}^r$ that describes reflection about the x_2-axis. The nonzero elements of $\boldsymbol{\Psi}^r$ are $\Psi^r_{11} = \Psi^r_{22} = \Psi^r_{33} = \Psi^r_{66} = 1$, $\Psi^r_{44} = \Psi^r_{55} = -1$. Note that $(\boldsymbol{\Psi}^r)^{-1} = \boldsymbol{\Psi}^r$. Apart from this difference in transformation matrices, the $\mathbf{D}_{\rho\beta}$ are found by a procedure that is analogous to that leading to (55), providing that the matrix $\boldsymbol{\Psi}$ is replaced by $\boldsymbol{\Psi}^r$. The result is

$$\mathbf{D}_{\rho\beta} = \boldsymbol{\Psi}^r\mathbf{D}_{\zeta\alpha}\boldsymbol{\Psi}^r, \qquad \alpha, \beta = 1, 2, \ldots N; \quad \rho, \zeta = 1, 2, \ldots M, \tag{57}$$

where $\mathbf{D}_{\zeta\alpha}$ was evaluated above in the x_j system, for unit eigenstrains in the subdomain A.

The same transformation relates the subset $\mathbf{D}_{\rho\gamma}$ for eigenstrains given in subdomain C to subset $\mathbf{D}_{\zeta\delta}$ in subdomain D, and the subset $\mathbf{D}_{\rho\varphi}$ for eigenstrains given in subdomain F to the subset $\mathbf{D}_{\zeta\varepsilon}$ in subdomain E.

As an example of such transformation, consider the matrix $\mathbf{D}_{\rho\beta}$, where Ω_ρ is any subelement volume in subdomain C, say Ω_γ. Clearly, the matrix $\mathbf{D}_{\gamma\beta}$ can be obtained using (57) as

$$\mathbf{D}_{\gamma\beta} = \Psi^r\mathbf{D}_{\delta\alpha}\Psi^r. \tag{58}$$

The eigenstress concentration factors $\mathbf{F}_{\rho\eta}$, $\rho, \eta = 1, 2, \ldots M$, are evaluated in a similar fashion. They can be also calculated from the $\mathbf{D}_{\rho\eta}$ factors found in (55) or (57), using Eq. (26_2).

5
Inelastic response

Once the transformation concentration factors are known, one can proceed with evaluation of the inelastic local fields. A specific constitutive relation must be adopted in Ω_η to connect the current values or rates of $\boldsymbol{\varepsilon}^{\text{in}}_\eta(t)$ or $\boldsymbol{\sigma}^{\text{re}}_\eta(t)$ to the history of $\boldsymbol{\sigma}_\eta(t-\tau)$ or $\boldsymbol{\varepsilon}_\eta(t-\tau)$, and $\theta(t-\tau)$, respectively. Assuming piecewise uniform fields in the local volumes, one can formally write such constitutive relations in the general form

$$\boldsymbol{\sigma}^{\text{re}}_\eta(t) = \mathbf{g}(\boldsymbol{\varepsilon}_\eta(t-\tau), \theta(t-\tau)) \qquad \boldsymbol{\varepsilon}^{\text{in}}_\eta(t) = \mathbf{f}(\boldsymbol{\sigma}_\eta(t-\tau), \theta(t-\tau)). \tag{59}$$

When substituted into (19) and (20), this provides the governing equations for the total local fields,

$$\boldsymbol{\varepsilon}_\rho(t) + \sum_{\eta=1}^{M}\mathbf{D}_{\rho\eta}\mathbf{M}_\eta\mathbf{g}(\boldsymbol{\varepsilon}_\eta(t-\tau), \theta(t-\tau)) = \mathbf{A}_\rho\boldsymbol{\varepsilon}(t) + \mathbf{a}_\rho\theta(t) \tag{60}$$

$$\boldsymbol{\sigma}_\rho(t) + \sum_{\eta=1}^{M}\mathbf{F}_{\rho\eta}\mathbf{L}_\eta\mathbf{f}(\boldsymbol{\sigma}_\eta(t-\tau), \theta(t-\tau)) = \mathbf{B}_\rho\boldsymbol{\sigma}(t) + \mathbf{b}_\rho\theta(t), \tag{61}$$

where the thermal concentration factor tensors are evaluated from (27).

The mechanical and transformation concentration factors depend only on elastic moduli and on local geometry. If those remain constant, the governing equations can be differentiated and used for

evaluation of stress and strain increments, or their time rates. In this manner, the inelastic deformation problem for any heterogeneous medium is reduced to evaluation of the various concentration factor tensors or matrices, and to solution of one of the Eqs. (60), (61) along the prescribed overall stress or deformation path.

6
Elastic-plastic systems

To illustrate a class of applications of the Eqs. (60) and (61), we examine the overall behavior and local fields in a heterogeneous medium with elastic-plastic phases. In particular, let the phase response under the locally uniform fields in V_r or Ω_η be represented by the constitutive relations

$$d\boldsymbol{\sigma}_r = \mathscr{L}_r(\boldsymbol{\varepsilon}_r - \boldsymbol{\beta}_r)\,d\boldsymbol{\varepsilon}_r + \ell_r(\boldsymbol{\varepsilon}_r - \boldsymbol{\beta}_r)\,d\theta \qquad d\boldsymbol{\varepsilon}_r = \mathscr{M}_r(\boldsymbol{\sigma}_r - \boldsymbol{\alpha}_r) + m_r(\boldsymbol{\sigma}_r - \boldsymbol{\alpha}_r)\,d\theta. \tag{62}$$

where $\mathscr{L}_r$ and $\mathscr{M}_r$ are the instantaneous stiffness and compliance tensors, and ℓ_r, m_r are the thermal stress and strain tensors that typically describe the consequence of a vairation of yield stress with temperature. The $\boldsymbol{\alpha}_r$ and $\boldsymbol{\beta}_r$ represent back stress and back strain that define the current centers of the yield and relaxation surfaces. All these tensors depend in some given form on the past deformation history, hence in an actual material the instantaneous magnitudes of their coefficients will vary within each local volume V_r or Ω_η. To prevent large errors in evaluation of the local response, it is advisable to choose material models that permit refined subdivisions of the representative volume.

Rewriting (59) as

$$d\boldsymbol{\sigma}_r^{\mathrm{re}} = \mathscr{L}_r^p\,d\boldsymbol{\varepsilon}_r + \ell_r^p\,d\theta \qquad d\boldsymbol{\varepsilon}_r^{\mathrm{in}} = \mathscr{M}_r^p\,d\boldsymbol{\sigma}_r + m_r^p\,d\theta \tag{63}$$

with

$$\mathscr{L}_r^p = \mathscr{L}_r - \mathbf{L}_r \qquad \ell_r^p = (\ell_r - \mathbf{l}_r)$$

$$\mathscr{M}_r^p = \mathscr{M}_r - \mathbf{M}_r \qquad m_r^p = (m_r - \mathbf{m}_r), \tag{64}$$

and substituting for the eigenstrain terms into (60) and (61), one finds the following two systems of equations for local fields in elastic-plastic heterogeneous media:

$$d\boldsymbol{\varepsilon}_\rho + \sum_{\eta=1}^{M} \mathbf{D}_{\rho\eta}\mathbf{M}_\eta\mathscr{L}_\eta^p\,d\boldsymbol{\varepsilon}_\eta = \mathbf{A}_\rho\,d\boldsymbol{\varepsilon} + \left(\mathbf{a}_\rho - \sum_{\eta=1}^{M}\mathbf{D}_{\rho\eta}\mathbf{M}_\eta\ell_\eta^p\right)d\theta \tag{65}$$

$$d\boldsymbol{\sigma}_\rho + \sum_{\eta=1}^{M} \mathbf{F}_{\rho\eta}\mathbf{L}_\eta\mathscr{M}_\eta^p\,d\boldsymbol{\sigma}_\eta = \mathbf{B}_\rho\,d\boldsymbol{\sigma} + \left(\mathbf{b}_\rho - \sum_{\eta=1}^{M}\mathbf{F}_{\rho\eta}\mathbf{L}_\eta m_\eta^p\right)d\theta. \tag{66}$$

In actual numerical solutions, one may reduce these to the matrix forms

$$\{d\boldsymbol{\varepsilon}_\rho\} = [\,\mathrm{diag}\,(\mathrm{I}) + [\mathbf{D}_{\rho\eta}\mathbf{M}_\eta\mathscr{L}_\eta^p]\,]^{-1}\{[\mathbf{A}_\rho]\,d\boldsymbol{\varepsilon} - [\mathbf{D}_{\rho\eta}\mathbf{M}_\eta]\{\mathbf{l}_\eta + \ell_\eta^p\}\,d\theta\} \tag{67}$$

$$\{d\boldsymbol{\sigma}_\rho\} = [\,\mathrm{diag}\,(\mathrm{I}) + [\mathbf{F}_{\rho\eta}\mathbf{L}_\eta\mathscr{M}_\eta^p]\,]^{-1}\{[\mathbf{B}_\rho]\,d\boldsymbol{\sigma} - [\mathbf{F}_{\rho\eta}\mathbf{L}_\eta]\{\mathbf{m}_\eta + m_\eta^p\}\,d\theta\}. \tag{68}$$

If one of these is solved for the local fields, then the overall response of the representative volume V follows from (5), (6) or (8), (9), and (10).

Of course, for rather coarse subdivisions of the microstructure, the governing equations can be solved in closed form. For example, in a two-phase system $r = \alpha, \beta$, or $\mathrm{M} = 2$ in (65) to (68), one can find the solution of these equations as (Dvorak 1991)

$$d\boldsymbol{\varepsilon}_r = \mathscr{A}_r\,d\boldsymbol{\varepsilon} + a_r\,d\theta \qquad d\boldsymbol{\sigma}_r = \mathscr{B}_r\,d\boldsymbol{\sigma} + \ell_r\,d\theta, \tag{69}$$

where, for $r = \alpha$,

$$\mathscr{A}_\alpha = [\mathrm{I} + \mathbf{D}_{\alpha\alpha}\mathbf{M}_\alpha\mathscr{L}_\alpha^p - (c_\alpha/c_\beta)\,\mathbf{D}_{\alpha\beta}\mathbf{M}_\beta\mathscr{L}_\beta^p]^{-1}[\mathbf{A}_\alpha - (1/c_\beta)\,\mathbf{D}_{\alpha\beta}\mathbf{M}_\beta\mathscr{L}_\beta^p]$$

$$a_\alpha = [\mathrm{I} + \mathbf{D}_{\alpha\alpha}\mathbf{M}_\alpha\mathscr{L}_\alpha^p - (c_\alpha/c_\beta)\,\mathbf{D}_{\alpha\beta}\mathbf{M}_\beta\mathscr{L}_\beta^p]^{-1}[\mathbf{a}_\alpha - \mathbf{D}_{\alpha\alpha}\mathbf{M}_\alpha\ell_\alpha^p - \mathbf{D}_{\alpha\beta}\mathbf{M}_\beta\ell_\beta^p] \tag{70}$$

$$\mathscr{B}_\alpha = [\mathrm{I} + \mathbf{F}_{\alpha\alpha}\mathbf{L}_\alpha\mathscr{M}_\alpha^p - (c_\alpha/c_\beta)\,\mathbf{F}_{\alpha\beta}\mathbf{L}_\beta\mathscr{M}_\beta^p]^{-1}[\mathbf{B}_\alpha - (1/c_\beta)\,\mathbf{F}_{\alpha\beta}\mathbf{L}_\beta\mathscr{M}_\beta^p]$$

$$\ell_\alpha = [\mathrm{I} + \mathbf{F}_{\alpha\alpha}\mathbf{L}_\alpha\mathscr{M}_\alpha^p - (c_\alpha/c_\beta)\,\mathbf{F}_{\alpha\beta}\mathbf{L}_\beta\mathscr{M}_\beta^p]^{-1}[\mathbf{b}_\alpha - \mathbf{F}_{\alpha\alpha}\mathbf{L}_\alpha m_\alpha^p - \mathbf{F}_{\alpha\beta}\mathbf{L}_\beta m_\beta^p]. \tag{71}$$

$\mathscr{A}_{\beta,\alpha\beta}$, etc., follow from an exchange of subscripts.

Once the local fields are known, the overall instantaneous response is described in analogy with (11) to (13) as

$$d\boldsymbol{\sigma} = \mathscr{L}\, d\boldsymbol{\varepsilon} + \ell\, d\theta \qquad d\boldsymbol{\varepsilon} = \mathscr{M} d\boldsymbol{\sigma} + m\, d\theta \tag{72}$$

$$\mathscr{L} = \sum_{r=1}^{M} c_r \mathscr{L}_r \mathscr{A}_r \qquad \ell = \sum_{r=1}^{M} c_r (\mathscr{L}_r a_r + \ell_r) \tag{73}$$

$$\mathscr{M} = \sum_{r=1}^{M} c_r \mathscr{M}_r \mathscr{B}_r \qquad m = \sum_{r=1}^{M} c_r (\mathscr{M}_r \ell_r + m_r). \tag{74}$$

As long as the transformation concentration factor tensors $\mathbf{D}_{\rho\eta}$ and $\mathbf{F}_{\rho\eta}$ satisfy the general relations (48) to (51), it can be established that (5) to (10) and (72) to (74) provide identical magnitudes of the overall instantaneous strain increments under given overall incremental stress and temperature changes.

The instantaneous overall properties (72) of multiphase aggregates, or unit cells subdivided into many elements, can be evaluated in a similar way. First, (69) are augmented for all volumes Ω_ρ, $\rho = 1, 2, \ldots M$, and written in matrix form as

$$\{d\boldsymbol{\varepsilon}_\rho\} = [\mathscr{A}_\rho]\, d\boldsymbol{\varepsilon} + \{a_\rho\}\, d\theta \qquad \{d\boldsymbol{\sigma}_\rho\} = [\mathscr{B}_\rho]\, d\boldsymbol{\sigma} + \{\ell_\rho\}\, d\theta. \tag{75}$$

Then, comparing (75_1) and (67), one finds the augmented instantaneous strain concentration factors $[\mathscr{A}_\rho]$ and the thermal strain concentration factors $\{a_\rho\}$ as

$$[\mathscr{A}_\rho] = [\,\mathrm{diag}(\mathbf{I}) + [\mathbf{D}_{\rho\eta}\mathbf{M}_\eta \mathscr{L}_\eta^p]\,]^{-1}[\mathbf{A}_\rho] \tag{76}$$

$$\{a_\rho\} = -[\,\mathrm{diag}(\mathbf{I}) + [\mathbf{D}_{\rho\eta}\mathbf{M}_\eta \mathscr{L}_\eta^p]\,]^{-1}\{[\mathbf{D}_{\rho\eta}\mathbf{M}_\eta]\{\mathbf{l}_\eta + \ell_\eta^p\}\}, \tag{77}$$

or, using (27),

$$\{a_\rho\} = [\,\mathrm{diag}(\mathbf{I}) + [\mathbf{D}_{\rho\eta}\mathbf{M}_\eta \mathscr{L}_\eta^p]\,]^{-1}\{\{\mathbf{a}_\rho\} - [\mathbf{D}_{\rho\eta}\mathbf{M}_\eta]\{\ell_\eta^p\}\}. \tag{78}$$

A substitution of (76) into (73) then provides the overall instantaneous stiffness matrix for the aggregate as

$$\{\mathscr{L}\} = [c_\rho \mathscr{L}_\rho]\,[\,\mathrm{diag}(\mathbf{I}) + [\mathbf{D}_{\rho\eta}\mathbf{M}_\eta \mathscr{L}_\eta^p]\,]^{-1}[\mathbf{A}_\rho]. \tag{79}$$

The instantaneous thermal stress matrix is found by substituting (77) or (78) into (73_2),

$$\{\ell\} = [c_\rho \mathscr{L}_\rho]\,[\,\mathrm{diag}(\mathbf{I}) + [\mathbf{D}_{\rho\eta}\mathbf{M}_\eta \mathscr{L}_\eta^p]\,]^{-1}\{\{\mathbf{a}_\rho\} - [\mathbf{D}_{\rho\eta}\mathbf{M}_\eta]\{\ell_\eta^p\}\} + \left\{\sum_{\eta=1}^{M} c_\eta \ell_\eta\right\}. \tag{80}$$

A similar procedure based on (68), (74_2) and (75_2) yields the overall instantaneous compliance matrix and the thermal strain matrix. The result is

$$\{\mathscr{M}\} = [c_\rho \mathscr{M}_\rho]\,[\,\mathrm{diag}(\mathbf{I}) + [\mathbf{F}_{\rho\eta}\mathbf{L}_\eta \mathscr{M}_\eta^p]\,]^{-1}[\mathbf{B}_\rho] \tag{81}$$

$$\{m\} = [c_\rho \mathscr{M}_\rho]\,[\,\mathrm{diag}(\mathbf{I}) + [\mathbf{F}_{\rho\eta}\mathbf{L}_\eta \mathscr{M}_\eta^p]\,]^{-1}\{\{\mathbf{b}_\rho\} - [\mathbf{F}_{\rho\eta}\mathbf{L}_\eta]\{m_\eta^p\}\} + \left\{\sum_{\eta=1}^{M} c_\eta m_\eta\right\}. \tag{82}$$

These expressions provide the overall instantaneous moduli and compliances that may be used in analysis of elastic-plastic composite structures, such as laminated plates and shells.

To illustrate the numerical results obtained from (68), we apply the above procedure to modeling of the elastic-plastic response of fibrous composites using the periodic hexagonal array (PHA) model described by Dvorak and Teply (1985) and Teply and Dvorak (1988). As shown in Fig. 2, the fibers are arranged in a hexagonal array and the fiber cross section is approximated by a 6 to 12-sided polygon. Higher order polygons are used with refined meshes, Figs. 4b and 5. The composite volume is then divided into shaded and unshaded triangular prisms. It has been shown in *op. cit.* that under overall uniform strain or stress applied to the model composite, one can derive certain periodic boundary conditions for the prisms that guarantee that the local stress and strain fields in the shaded and unshaded prisms are related by a simple coordinate transformation; hence one of the prisms can be selected as

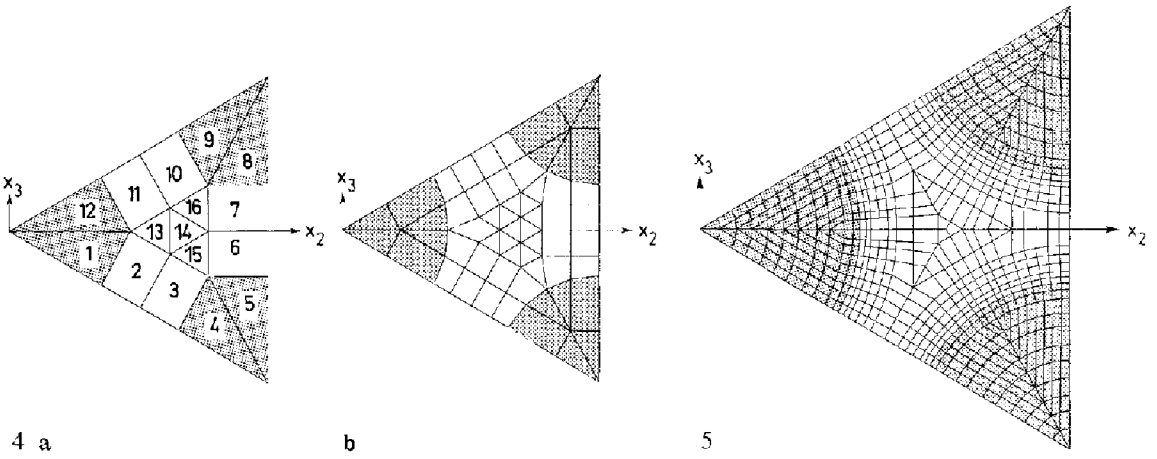

4 a b 5

Figs. 4–5. 4 Examples of finite element meshes in the unit cell of the PHA model. 5 A refined finite element mesh in the unit cell of the PHA model

the representative unit cell of the fibrous composite. Figure 3 shows the geometry of the unit cell for a hexagonal fiber. The finite element meshes that may be selected in the cell are illustrated by the examples shown in Figs. 4 and 5. The calculations reported here were performed with the crude mesh of Fig. 4a.

In preparation for the numerical solution of (68), the element concentration factor matrices $\mathbf{B}_\rho$ and the influence functions $\mathbf{F}_{\rho\eta}$ were evaluated according to the procedure outlined in Sect. 4.1. In fact, a slight modification of the procedure yields directly the matrix multiplication $(\mathbf{F}_{\rho\eta}\mathbf{L}_\eta)$. Indeed, if one rewrites (20) as

$$\boldsymbol{\sigma}_\rho(t) = \mathbf{B}_\rho\,\boldsymbol{\sigma}(t) - \sum_{\eta=1}^{M} (\mathbf{F}_{\rho\eta}\mathbf{L}_\eta)\,\boldsymbol{\mu}_\eta(t), \tag{83}$$

where t indicates the locations on the loading path $\boldsymbol{\sigma}(t)$, then the columns of the matrix $(\mathbf{F}_{\rho\eta}\mathbf{L}_\eta)$ can be identified with the local stresses caused in Ω_ρ by a uniform unit eigenstrain $\boldsymbol{\mu}_\eta = -\mathbf{i}_k$, $k = 1, 2, \ldots 6$, applied in Ω_η, while the composite aggregate is free of any overall stress $\boldsymbol{\sigma}(t) = 0$. These local stresses can be found from (30), where the strains $\boldsymbol{\varepsilon}_\eta$ follow from a solution of (37)–(44).

In the present example, Eqs. (37)–(44) were formed and solved with the ABAQUS finite element program. In more refined meshes, the magnitude of several influence coefficients $\mathbf{F}_{\rho\eta}$, $\rho \neq \eta$, may be found to be small in comparison with the coefficients $\mathbf{F}_{\rho\rho}$, particularly when the element ρ is far removed from the element η which contains the unit eigenstrain. Of course, all influence coefficients should be computed, but some products $\mathbf{F}_{\rho\eta}\mathbf{L}_\eta\mathscr{M}^p_\eta$ in (81), (82) may be discarded if the transmitted contribution of the eigenstrain present in element Ω_η to the strain in element Ω_ρ are small in comparison with the total strain in Ω_ρ.

The piecewise uniform local stress field was found by integration of (68) along the thermomechanical loading path specified by the history of overall stress $\boldsymbol{\sigma}^0(t)$ and temperature $\theta^0(t)$. The Runge-Kutta formula of order two was used in the solution. The instantaneous plastic compliance matrix $\mathscr{M}^p_\eta$, the thermal strain matrix $\mathscr{m}^p_\eta$, as well as the element strains $\boldsymbol{\varepsilon}_\eta$, $\eta = 1, 2, \ldots M$, were evaluated for the elements in the elastic-plastic matrix phase, with the constitutive equations summarized in Appendix A. The overall strain was then found from (8_1).

The solution algorithm for elastic-plastic composites may be constructed as follows.

Step 1: For the given interval $t_1 \leqq t \leqq t_{n+1}$ of the prescribed histories $\boldsymbol{\sigma}^0(t)$ and $\theta^0(t)$, select the number of increments n, and compute the time increment $h = (t_{n+1} - t_1)/n$.

Step 2: Set the initial values of the stress field $\boldsymbol{\sigma}_\rho(t_1) = \hat{\boldsymbol{\sigma}}_\rho$, the strain field $\boldsymbol{\varepsilon}_\rho(t_1) = \hat{\boldsymbol{\varepsilon}}_\rho$, of the center of the yield surface $\boldsymbol{\alpha}_\rho(t_1) = \hat{\boldsymbol{\alpha}}_\rho$, (Appendix A), and of the tensile yield stress $Y_\rho(t_1) = \hat{Y}_\rho$, in the elements $\rho = 1, 2, \ldots M$.

Step 3: For $k = 1, 2, \ldots n$, do steps 4–6.

Step 4: Compute the yield function $g^{(k)}_\rho(\boldsymbol{\sigma}^{(k)}_\rho - \boldsymbol{\alpha}^{(k)}_\rho, \theta_k)$ in Appendix A.

Step 5: If $g^{(k)}_\rho < 0 \Rightarrow$ volume Ω_ρ is elastic; go to step 6,
if $g^{(k)}_\rho = 0$, compute $\{d\boldsymbol{\sigma}_\rho\}_k$ from (68), with $d\boldsymbol{\sigma}$ replaced by $d\boldsymbol{\sigma}^0(t_k)$ and $d\theta$ is replaced by $d\theta^0(t_k)$:
If $(\partial g_\rho/\partial\boldsymbol{\sigma}_\rho)_k \cdot (d\boldsymbol{\sigma}_\rho)_k \leqq 0 \Rightarrow$ elastic unloading; go to step 6,
If $(\partial g_\rho/\partial\boldsymbol{\sigma}_\rho)_k \cdot (d\boldsymbol{\sigma}_\rho)_k > 0 \Rightarrow$ plastic loading; compute the instantaneous plastic compliance and thermal strain vectors $\mathscr{M}^p_\rho(\boldsymbol{\sigma}^{(k)}_\rho - \boldsymbol{\alpha}^{(k)}_\rho, \theta_k)$, $\mathscr{m}^p_\rho(\boldsymbol{\sigma}^{(k)}_\rho - \boldsymbol{\alpha}^{(k)}_\rho, \theta_k)$, Appendix A.

Step 6: Compute the stress field at time t_{k+1}:

$$\{\boldsymbol{\sigma}_\rho\}_{k+1} = \{\boldsymbol{\sigma}_\rho\}_k + (h/2)\{d\boldsymbol{\sigma}_\rho + d\boldsymbol{\sigma}_\rho^*\}_k,$$

$$\{d\boldsymbol{\sigma}_\rho^*\}_k = \{d\boldsymbol{\sigma}_\rho(t_{k+1}, \{\boldsymbol{\sigma}_\rho\}_k + h\{d\boldsymbol{\sigma}_\rho\}_k)\},$$

where $d\boldsymbol{\sigma}_\rho^*(t, \boldsymbol{\sigma}_\rho)$ follow from (68) using an adjusted stress. The corresponding strain, $\boldsymbol{\varepsilon}_\rho(t_{k+1})$, $\rho = 1, 2, \ldots M$, and the center of yield surface $\boldsymbol{\alpha}_\rho(t_{k+1})$, $\rho = 1, 2, \ldots T$, are found from the constitutive equations given in Appendix A; T is the number of the elastic-plastic element volumes at time t_k.

The solution depends on the selected magnitude of the time increment h; an error of order h^2 is expected in the Runge-Kutta formula used. Our implementation of the above algorithm included iterations with various magnitudes of the time increment h. Specifically, the solution found at time t_{n+1} for the selected number of time intervals n, was compared to the solution found when the number of time increments was increased to $2n$. The solutions were compared in terms of the magnitude $\|\{\boldsymbol{\sigma}_\rho\}\|$ of the stress vector. If the absolute difference $(\|\{\boldsymbol{\sigma}_\rho\}\|_{n+1} - \|\{\boldsymbol{\sigma}_\rho\}\|_{2n+1}) > \gamma$, a specified tolerance, the process was repeated with the number of time intervals doubled again. Consequently, a series of solutions corresponding to time intervals $n, 2n, 4n, 8n, \ldots$ etc., was generated until the selected convergence criterion was satisfied. Other solution strategies may be employed as well, for example, the time increment may be adjusted according to a specified tolerance (Sloan 1987).

In the numerical example, we selected a boron/aluminum composite. The fiber is assumed to remain elastic during deformation, the elastic properties are chosen as $E = 379.2$ GPa and $\nu = 0.21$. The matrix elastic constants are taken as $E = 68.9$ GPa and $\nu = 0.33$, and its initial yield stress in simple tension as $Y = 24$ MPa. The Mises yield condition is used together with the Prager-Ziegler kinematic hardening rule. Linear hardening was assumed for the matrix with the plastic tangent modulus $H = 14$ GPa.

The composite model was first subjected to mechanical tensile loading along the overall stress path from $\sigma_{22} = 0$ to $\sigma_{22} = 100$ MPa. This was followed by unloading to $\sigma_{22} = 0$: the selected x_2-direction in the cartesian coordinate system is indicated in Fig. 3, x_1 coincides with the fiber axis. Response of the unit cell to the same loading path was also evaluated directly, using the standard elastic-plastic finite element (FE) procedure of the ABAQUS program. Similar calculations were performed for the transverse shear path from $\sigma_{23} = 0$ to $\sigma_{23} = 100$ MPa, followed by unloading to $\sigma_{23} = 0$. For both loading sequences, the overall total strains found using the transformation field analysis form (68) and the ABAQUS program were essentially identical; Fig. 6. All these solutions were based on the same number of load increments, selected as 40. Table 1 shows a comparison of the final magnitudes of local stresses σ_{22} computed in the elements of the coarse mesh, Fig. 4a, at the end of the transverse tension path ($\sigma_{22} = 0$). The local stresses σ_{23} computed in the elements at the end of the transverse shear path ($\sigma_{23} = 0$) are compared in Table 2. Tables 3 and 4 show the corresponding plastic strain components ε_{22}^p and ε_{23}^p in the matrix elements.

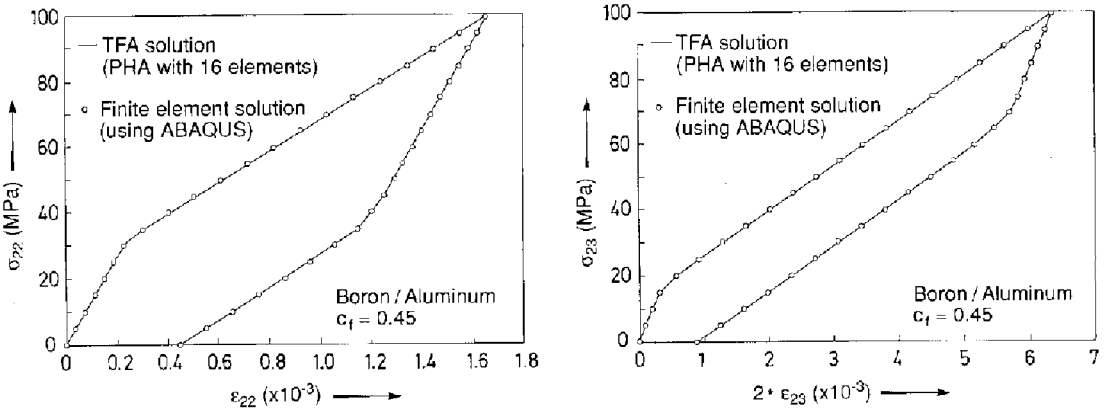

Fig. 6. Overall stress-strain predictions found with the finite element and TFA methods for an elastic-plastic B/Al composite under transverse tension loading and transverse shear loading

Table 1. Element stress σ_{22} computed at the end of an overall transverse tension cycle $\sigma_{22} = 0 \rightarrow 100 \rightarrow 0$ MPa

Element No. in Fig. 4a	FE Solution by ABAQUS (MPa)	TFA Solution (MPa)	% Difference‡
(fiber)			
1	1.90183214667	1.82551033611	4.01
4	−3.81085837097	−3.82716055068	0.43
5	11.8557301133	11.7818613295	0.62
(matrix)			
2	−13.643539477	−13.6495023486	0.04
3	21.2004259013	21.1675381753	0.16
6	−13.7264248309	−13.598549014	0.93
13	19.0704404461	19.2641299257	1.02
14	−14.5503830631	−14.3651255519	1.27
15	−13.0342676901	−13.0052217598	0.22

‡ ((ABAQUS magnitude − TFA magnitude)/(ABAQUS magnitude)) × 100

Table 2. Element stress σ_{23} computed at the end of an overall transverse shear cycle $\sigma_{23} = 0 \rightarrow 100 \rightarrow 0$ MPa

Element No. in Fig. 4a	FE Solution by ABAQUS (MPa)	TFA Solution (MPa)	% Difference‡
(fiber)			
1	8.08962648043	8.03538699975	0.67
4	4.38705814316	4.134745415385	0.90
5	0.74283546995	0.741202776042	0.22
(matrix)			
2	−1.64170439373	−1.64972131814	0.49
3	−4.37508035553	−4.34663883063	0.65
6	−4.94752990238	−4.91791139298	0.60
13	0.464416136927	0.472410022578	1.72
14	−5.18859682347	−4.94389812139	4.72
15	−4.44559853765	−4.44358475334	0.05

‡ ((ABAQUS magnitude − TFA magnitude)/(ABAQUS magnitude)) × 100

Table 3. Matrix plastic normal strain ε_{22}^{p} computed at the end of an overall transverse tension cycle $\sigma_{22} = 0 \rightarrow 100 \rightarrow 0$ MPa

Element No. in Fig. 4a	FE Solution by ABAQUS (10^{-6})	TFA Solution (10^{-6})	% Difference‡
2	537.233705579	533.306741197	0.73
3	1153.37261718	1154.15883461	0.07
6	1151.97490964	1152.98182129	0.09
13	276.016801092	271.873804193	1.50
14	−47.4017857507	−50.2394881913	5.99
15	1158.02013150	1158.16415196	0.01

‡ ((ABAQUS magnitude − TFA magnitude)/(ABAQUS magnitude)) × 100

To compare the efficiency of the TFA method with that of the ABAQUS (version 4.8) finite element solution, we recorded the respective CPU computing times required in the two load cycles using a VAX mainframe computer system. Under the transverse tension cycle, the ABAQUS solution required 204 s while the TFA solution required 67 s. For the transverse shear loading cycle, the CPU times for the ABAQUS solution and the TFA method were 263 s and 67 s, respectively. Additional time was required to obtain the stress concentration factors $\mathbf{B}_{\rho}$, $\rho = 1, 2, \ldots M$, and the transformation coefficients $(\mathbf{F}_{\rho\eta}\mathbf{L}_{\eta})$, $\rho = 1, 2, \ldots M$, $\eta = 1, 2, \ldots T$, Eq. (83), where M is the total number of subvolumes in the unit cell and

Table 4. Matrix plastic shear strain $2\varepsilon_{23}^{p}$ computed at the end of an overall transverse shear cycle $\sigma_{23} = 0 \rightarrow 100 \rightarrow 0$ MPa

Element No. in Fig. 4a	FE Solution by ABAQUS (10^{-6})	TFA Solution (10^{-6})	% Difference‡
2	2591.29732547	2590.42812482	0.03
3	1368.39041486	1363.58835703	0.35
6	1820.69087664	1827.88019543	0.40
13	3068.74769946	3070.46067496	0.06
14	−708.059347361	−724.462785666	2.32
15	824.209068909	820.199975761	0.49

‡ ((ABAQUS magnitude − TFA magnitude)/(ABAQUS magnitude)) × 100

Table 5. Element stresses σ_{22} and σ_{23} computed at the end of the loading path of Fig. 7

Element No.*	σ_{22} (MPa)			σ_{23} (MPa)		
	ABAQUS	TFA	% Difference‡	ABAQUS	TFA	% Difference‡
(fiber)						
1	2.486314943	2.484838314	0.06	6.199577168	6.196482812	0.05
4	−2.496518548	−2.495716646	0.03	2.734338180	2.732595877	0.06
(matrix)						
2	−15.19959704	−15.19599072	0.02	−1.4786011859	−1.478106587	0.03
3	−0.237086563	−0.233915256	1.34	4.923139542	−4.922870483	0.01
13	3.6118504320	3.597884176	0.39	0.508403072	0.508454116	0.01
15	−34.97372735	−34.96793825	0.02	−5.455541995	−5.455215211	0.01

* See Fig. 4a

‡ ((ABAQUS magnitude − TFA magnitude)/(ABAQUS magnitude)) × 100

Table 6. Matrix plastic strains ε_{22}^{p} and $2\varepsilon_{23}^{p}$ computed at the end of the loading path of Fig. 7

Element No.*	ε_{22}^{p} (10^{-6})			$2\varepsilon_{23}^{p}$ (10^{-6})		
	ABAQUS	TFA	% Difference‡	ABAQUS	TFA	% Difference‡
2	−14.2658225	−14.2675437	0.01	2612.04123	2612.15041	0.004
3	−945.3500971	−945.4331740	0.01	1378.96867	1378.97982	0.001
13	−7.6954323	7.5805950	1.49	3077.51206	3077.52259	0.000
15	−1014.387728	−1014.377705	0.001	599.29864	599.43807	0.020

* See Fig. 4a

‡ ((ABAQUS magnitude − TFA magnitude)/(ABAQUS magnitude)) × 100

T is the number of matrix elements. As described in Sect. 4.1, the coefficients of the stress concentration factors $\mathbf{B}_{\rho}$ are found from solutions of six successive elasticity problems, and the coefficients of the transformation coefficients $(\mathbf{F}_{\rho\eta}\mathbf{L}_{\eta})$ are found from solutions of $6T$ succesive elasticity problems. Considering the mesh of Fig. 4a with $M = 16$, $T = 10$, a total of 66 elasticity problems were solved to compute the required coefficients. Each problem registered 3s of CPU time on the VAX computer for a total of 198s. However, this is a one time operation for a given mesh. In any case, substantial savings in the computing time were realized by the TFA method in these examples.

Another comparison of the elastic-plastic response computed with the TFA and FE methods was made for the mesh of Fig. 4a and a complex loading path in the $\sigma_{22}\sigma_{23}$-stress space, Fig. 7. Figures 8 and 9 show the overall stress-strain response computed with the TFA method where the numbered symbols correspond to the loading points indicated in Fig. 7. The local stresses and plastic strains found with the TFA and the FE methods at the end of the loading path are compared in Tables 5 and 6, respectively, for selected elements.

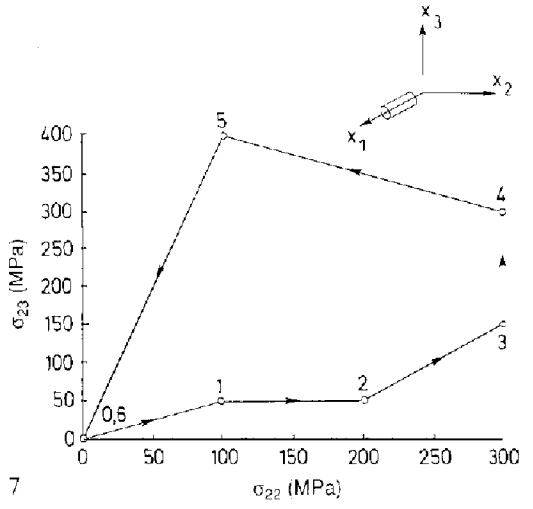

7

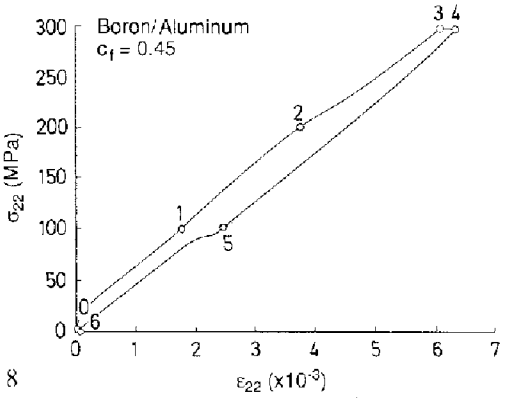

8

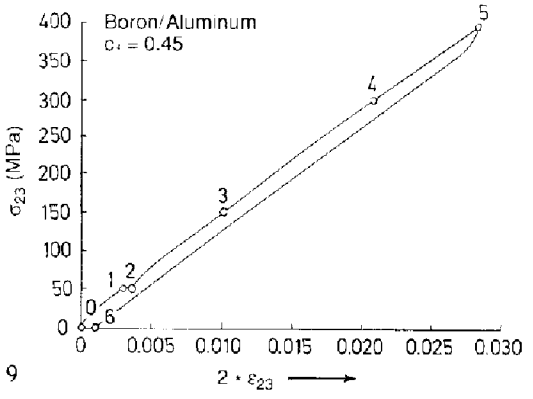

9

Figs. 7–9. 7 Transverse tension-transverse shear stress path applied to an elastic-plastic B/Al composite. 8 Overall $\sigma_{22} - \varepsilon_{22}$ response predicted by the TFA method for the loading path of Fig. 7. 9 Overall $\sigma_{22} - \varepsilon_{22}$ response predicted by the TFA method for the loading path of Fig. 7

We recall from Sect. 4.2 that the number of operations depends on the number of elements. Therefore, the efficiency of the two methods must be compared with regard to the mesh refinement in the solution domain.

The cost of both the TFA and the FE solutions depends on many other factors, such as the specified tolerance and the number of iterations required to achieve such tolerance. More exact comparisons of the efficiency of the two methods can be made only for actual applications.

Note also that the TFA method can readily use any selected constitutive equation for the phases, whereas a separate UMAT routine would be needed for implementation of such equations into the ABAQUS program.

7
Viscoelastic systems

It is well-known that the correspondence principle in linear viscoelasticity can be used to relate the effective viscoelastic properties of a composite medium to the effective elastic properties (Christensen 1971, 1979). However, the procedure often requires an analytic elasticity solution, and after this is converted into a transform-parameter multiplied Laplace or Fourier transform of the viscoelasticity solution, an inversion is needed for the transformed solution.

The present approach avoids the difficulties involved, and is applicable not only to linear, but also to nonlinear viscoelastic phases. For a history of applied stress that starts from zero stress at $t = 0$, the phase constitutive equations are taken in the form

$$\varepsilon_r(t) = \int_0^t \mathbf{J}_r(t-\tau)\frac{d\boldsymbol{\sigma}_r(\tau)}{d\tau}d\tau, \tag{84}$$

where $\mathbf{J}_r(t-\tau)$ is the creep compliance, with assumed symmetries $J^r_{ijkl} = J^r_{jikl} = J^r_{ijlk} = J^r_{klij}$. We also assume the existence of a nonvanishing compliance $\mathbf{J}_r(0)$ that defines the instantaneous elastic response, and thus provides property magnitudes needed in evaluation of the transformation influence functions.

Similarly, for a history of local strain starting at zero strain at $t = 0$, the total stresses are given by

$$\boldsymbol{\sigma}_r(t) = \int_0^t \mathbf{G}_r(t-\tau)\frac{d\boldsymbol{\varepsilon}_r(\tau)}{d\tau}\,d\tau, \tag{85}$$

where $\mathbf{G}_r(t-\tau)$ is the local relaxation function with the same symmetries that were indicated for $\mathbf{J}_r(t-\tau)$, and $\mathbf{G}_r(0) \neq \mathbf{0}$ describes the elastic response.

The corresponding rates are obtained from the above relations as

$$\dot{\boldsymbol{\varepsilon}}_r(t) = \mathbf{M}_r\,\dot{\boldsymbol{\sigma}}_r(t) + \dot{\mathbf{J}}_r(0)\,\boldsymbol{\sigma}_r(t) + \int_0^t \ddot{\mathbf{J}}_r(t-\tau)\,\boldsymbol{\sigma}_r(\tau)\,d\tau, \tag{86}$$

$$\dot{\boldsymbol{\sigma}}_r(t) = \mathbf{L}_r\,\dot{\boldsymbol{\varepsilon}}_r(t) + \dot{\mathbf{G}}_r(0)\,\boldsymbol{\varepsilon}_r(t) + \int_0^t \ddot{\mathbf{G}}_r(t-\tau)\,\boldsymbol{\varepsilon}_r(\tau)\,d\tau. \tag{87}$$

The elastic and inelastic parts of the total strain and stress, and of the respective rates, are easily separated, and the latter are substituted into appropriate total or rate forms of (19), (20), or (60), (61). For example, if the composite is loaded by a history of overall stress $\boldsymbol{\sigma}^0(t)$ and temperature history $\theta^0(t)$, the local stresses and their rates follow from

$$\dot{\boldsymbol{\sigma}}_\rho(t) = \mathbf{B}_\rho\,\dot{\boldsymbol{\sigma}}^0(t) - \sum_{\eta=1}^{M} \mathbf{F}_{\rho\eta}\mathbf{L}_\eta\left\{\mathbf{m}_\eta\,\dot{\theta}^0(t) + \dot{\mathbf{J}}_\eta(0)\,\boldsymbol{\sigma}_\eta(t) + \int_0^t \ddot{\mathbf{J}}_\eta(t-\tau)\,\boldsymbol{\sigma}_\eta(\tau)\,d\tau\right\}. \tag{88}$$

The terms on the right of (88) are functions of the current state and applied load. Integration of (88) along a specified loading path yields the local stresses in the local volumes Ω_ρ, $\rho = 1, 2, \ldots M$. The corresponding strains are found by integration of (86). Again, the columns of matrix $(\mathbf{F}_{\rho\eta}\mathbf{L}_\eta)$, ρ, $\eta = 1, 2, \ldots M$, are identified with the local stresses caused in Ω_ρ by a uniform eigenstrain $\boldsymbol{\mu} = \mathbf{i}_k$, $k = 1, 2, \ldots 6$, applied in Ω_η while the overall stress $\boldsymbol{\sigma}(t)$ vanish, as suggested by Eq. (83).

In addition to the relations (88) for the stress rates, one can also find governing equations for the total local stresses. The elastic strain is subtracted from the total strain in (84) and the resulting inelastic strain is substituted into (61). The result is

$$\boldsymbol{\sigma}_\rho(t) = \mathbf{B}_\rho\,\boldsymbol{\sigma}^0(t) - \sum_{\eta=1}^{M} \mathbf{F}_{\rho\eta}\mathbf{L}_\eta\left\{\mathbf{m}_\eta\,\theta^0(t) - \mathbf{M}_\eta\,\boldsymbol{\sigma}_\eta(t) + \int_0^t \mathbf{J}_\eta(t-\tau)\,(d\boldsymbol{\sigma}_\eta(\tau)/d\tau)\,d\tau\right\}. \tag{89}$$

Particularly simple relations for the local fields can be written in two-phase systems, subdivided into only two local volumes $r = \alpha, \beta$. In this case, differentiation of (60) provides

$$\begin{aligned}
&\dot{\boldsymbol{\varepsilon}}_\alpha(t) + \mathbf{D}_{\alpha\alpha}\mathbf{M}_\alpha\,\dot{\boldsymbol{\sigma}}_\alpha^{re}(t) + \mathbf{D}_{\alpha\beta}\mathbf{M}_\beta\,\dot{\boldsymbol{\sigma}}_\beta^{re}(t) = \mathbf{A}_\alpha\,\dot{\boldsymbol{\varepsilon}}(t) + \mathbf{a}_\alpha\,\dot{\theta}(t)\\
&\dot{\boldsymbol{\varepsilon}}_\beta(t) + \mathbf{D}_{\beta\alpha}\mathbf{M}_\alpha\,\dot{\boldsymbol{\sigma}}_\alpha^{re}(t) + \mathbf{D}_{\beta\beta}\mathbf{M}_\beta\,\dot{\boldsymbol{\sigma}}_\beta^{re}(t) = \mathbf{A}_\beta\,\dot{\boldsymbol{\varepsilon}}(t) + \mathbf{a}_\beta\,\dot{\theta}(t).
\end{aligned} \tag{90}$$

This can be easily solved; note that according to (51_1) there is

$$\begin{aligned}
&c_\alpha\mathbf{D}_{\alpha\alpha} + c_\beta\mathbf{D}_{\beta\alpha} = \mathbf{0} \Rightarrow \mathbf{D}_{\alpha\alpha} = -(c_\beta/c_\alpha)\mathbf{D}_{\beta\alpha}, \quad \mathbf{D}_{\beta\alpha}\mathbf{D}_{\alpha\alpha} = -(c_\beta/c_\alpha)\mathbf{D}_{\beta\alpha}\mathbf{D}_{\beta\alpha} = \mathbf{D}_{\alpha\alpha}\mathbf{D}_{\beta\alpha},\\
&\dot{\boldsymbol{\varepsilon}} = c_\alpha\dot{\boldsymbol{\varepsilon}}_\alpha + c_\beta\dot{\boldsymbol{\varepsilon}}_\beta \Rightarrow \dot{\boldsymbol{\varepsilon}}_\alpha = (\dot{\boldsymbol{\varepsilon}} - c_\beta\dot{\boldsymbol{\varepsilon}}_\beta)/c_\alpha.
\end{aligned} \tag{91}$$

Then, after some algebra one finds the following equation for the local strain rate in one phase, say $r = \beta$,

$$\begin{aligned}
[\mathbf{D}_{\alpha\alpha} + (c_\beta/c_\alpha)\mathbf{D}_{\beta\alpha}]\,\dot{\boldsymbol{\varepsilon}}_\beta(t) = {}& (\mathbf{D}_{\beta\alpha}\mathbf{D}_{\alpha\beta} - \mathbf{D}_{\alpha\alpha}\mathbf{D}_{\beta\beta})\mathbf{J}_\beta(0)\,\dot{\mathbf{G}}_\beta(0)\,\boldsymbol{\varepsilon}_\beta(t)\\
&+ (\mathbf{D}_{\beta\alpha}\mathbf{D}_{\alpha\beta} - \mathbf{D}_{\alpha\alpha}\mathbf{D}_{\beta\beta})\mathbf{J}_\beta(0)\int_0^t \ddot{\mathbf{G}}_\beta(t-\tau)\,\boldsymbol{\varepsilon}_\beta(\tau)\,d\tau\\
&- [\mathbf{D}_{\beta\alpha}(\mathbf{A}_\alpha - (1/c_\alpha)\mathbf{I}) - \mathbf{D}_{\alpha\alpha}\mathbf{A}_\beta]\,\dot{\boldsymbol{\varepsilon}}^0(t) - (\mathbf{D}_{\beta\alpha}\mathbf{a}_\alpha - \mathbf{D}_{\alpha\alpha}\mathbf{a}_\beta)\,\dot{\theta}^0(t).
\end{aligned} \tag{92}$$

A similar procedure involving total fields rather than rates gives the total local strain in the phase β as

$$[\mathbf{D}_{\alpha\alpha} + (c_\beta/c_\alpha)\mathbf{D}_{\beta\alpha}]\,\boldsymbol{\varepsilon}_\beta(t) = (\mathbf{D}_{\beta\alpha}\mathbf{D}_{\alpha\beta} - \mathbf{D}_{\alpha\alpha}\mathbf{D}_{\beta\beta})\mathbf{J}_\beta(0)\int_0^t \mathbf{G}_\beta(t-\tau)\,(d\boldsymbol{\varepsilon}_\beta(\tau)/d\tau)\,d\tau$$

$$-[\mathbf{D}_{\beta\alpha}(\mathbf{A}_\alpha - (1/c_\alpha)\mathbf{I}) - \mathbf{D}_{\alpha\alpha}\mathbf{A}_\beta]\,\boldsymbol{\varepsilon}^0(t) - (\mathbf{D}_{\beta\alpha}\mathbf{a}_\alpha - \mathbf{D}_{\alpha\alpha}\mathbf{a}_\beta)\,\theta^0(t). \tag{93}$$

The total stress fields, or strain fields, can be found at a given time t by solving the system of nonlinear Eqs. (89) or (93). Either the Newton's method or the fixed point solution may be used. Both methods require repeated evaluation of the nonlinear functions $\mathbf{J}_\eta$ in (89), or $\mathbf{G}_\beta$ in (93), and of the time derivative of the stress or strain fields. Moreover, Newton's method requires an evaluation of a Jacobian matrix from the nonlinear functions in (89) and (93), and of its inverse. This complicates the numerical procedure for evaulation of the local fields, and thus argues against writing the governing equations in the total form.

A more convenient and efficient procedure for evaluation of local fields is given by integration of the governing rate Eqs. (88) or (92). This involves evaluation of the integrands $[\dot{\mathbf{J}}_\eta(t-\tau)\,\boldsymbol{\sigma}_\eta(\tau)\,d\tau]$ or $[\dot{\mathbf{G}}_\eta(t-\tau)\,\boldsymbol{\varepsilon}_\eta(\tau)\,d\tau]$, $\eta = 1, 2, \ldots M$, from $\tau = 0$ to $\tau = t$. The local stress and strain histories are known up to the current time t, while derivatives of the creep compliance $\dot{\mathbf{J}}$ and of the relaxation function $\dot{\mathbf{G}}$ must be provided by the viscoelastic phase model. The local fields at time $(t + \Delta t)$ are then found by integration of the differential Eqs. (88) or (92), using for example the Runge-Kutta formula of order two, for specified histories of the overall stress rate $\dot{\boldsymbol{\sigma}}^0(t)$ or the overall strain rate $\dot{\boldsymbol{\varepsilon}}^0(t)$, and the temperature $\dot{\theta}^0(t)$. The solution algorithm for (88) then is

Step 1: Select the number of time increments, n, and compute the time increment $h = (t_{n+1} - t_1)/n$, where $t_1 = 0$ and t_{n+1} define the time interval in which the histories $\boldsymbol{\sigma}^0(t)$ and $\theta^0(t)$ are described.

Step 2: Set initial values of the local stress field as $\boldsymbol{\sigma}_\rho(t_1) = 0$, and of the local strain field $\boldsymbol{\varepsilon}_\rho(t_1) = 0$, and of the creep compliance $\mathbf{J}_\rho(0)$, $\rho = 1, 2, \ldots M$, using, for example, the four-parameter model (see Appendix B).

Step 3: For $k = 1, 2, \ldots n$, do steps 4, 5:

Step 4: Approximate the integral $\int_0^t \dot{\mathbf{J}}_{\eta}(t-\tau)\,\boldsymbol{\sigma}_\eta(\tau)\,d\tau$ by one of the closed Newton-Cotes formulas. For example, if the trapezoidal rule is used for each time increment, then

$$\int_0^t \dot{\mathbf{J}}_\eta(t-\tau)\,\boldsymbol{\sigma}_\eta(\tau)\,d\tau = \frac{h}{2}\sum_{j=1}^{k-1}[\dot{\mathbf{J}}_\eta(t_k - t_j)\,\boldsymbol{\sigma}_\eta(t_j) + \dot{\mathbf{J}}_\eta(t_k - t_{j-1})\,\boldsymbol{\sigma}_\eta(t_{j+1})].$$

Step 5: Compute the stress field at time t_{k+1}:

$$\{\boldsymbol{\sigma}_\rho\}_{k+1} = \{\boldsymbol{\sigma}_\rho\}_k + (h/2)\{\dot{\boldsymbol{\sigma}}_\rho + \dot{\boldsymbol{\sigma}}^*_\rho\}_k, \quad \{\dot{\boldsymbol{\sigma}}^*_\rho\}_k = \{\dot{\boldsymbol{\sigma}}_\rho(t_{k+1}, \{\boldsymbol{\sigma}_\rho\}_k + h\{\dot{\boldsymbol{\sigma}}_\rho\}_k)\},$$

where $\dot{\boldsymbol{\sigma}}^*_\rho(t, \boldsymbol{\sigma}_\rho)$ follow from the functional on the right of (88) using adjusted stress. The corresponding strain $\boldsymbol{\varepsilon}_\rho(t_{k-1})$, $\rho = 1, 2, \ldots M$, follows from (86).

Once again, the solution depends on the selected magnitude of the increment h, and an error of order h^3 is expected in the integration of step 4, and an error of order h^2 in the integration scheme of step 5. As in the elastic-plastic case, our implementation of the above algorithm included a convergence test in which the solution found at time t_{n+1} for a selected number of time intervals n was compared to the solution found when the number of time increments was increased to $2n$. If the absolute difference $(\|\{\boldsymbol{\sigma}_\rho\}\|_{n-1} - \|\{\boldsymbol{\sigma}_\rho\}\|_{2n+1}) > \gamma$, a specified tolerance, then the process was repeated with the number of time intervals multiplied again by a factor of two. Consequently a series of solutions corresponding to time intervals $n, 2n, 4n, 8n, \ldots$ etc., was generated until the selected convergence criterion was satisfied.

To provide an illustrative example, we examined the response of a glass/ED-6 resin composite with elastic fibers and viscoelastic matrix under both constant and cyclic stresses. Viscoelastic response of the matrix was determined from a four-parameter model consisting of Maxwell and Voigt elements in series. If the E^M and η^M denote the stiffness and viscosity parameters associated with the Maxwell element, and E^V, η^V the parameters associated with the Voigt element, then the uniaxial creep compliance function

for the four-parameter model is (Findley 1976)

$$J_A(t) = \frac{1}{E^M} + \frac{1}{E^V}\left[1 - \exp\left(-\frac{E^V t}{\eta^V}\right)\right] + \frac{t}{\eta^M}. \tag{94}$$

Derivation of a three-dimensional creep compliance function $\mathbf{J}(t)$ for the four-parameter model is given in Appendix B. When the result is substituted into (88), one finds the following differential equation for evaluation of the local stresses caused by the overall stress rate $\dot{\boldsymbol{\sigma}}^0(t)$ and temperature rate $\dot{\theta}^0(t)$:

$$\dot{\boldsymbol{\sigma}}_\rho(t) = \mathbf{B}_\rho \dot{\boldsymbol{\sigma}}^0(t) - \sum_{\eta=1}^{M} \mathbf{F}_{\rho\eta}\mathbf{L}_\eta \left\{ \mathbf{m}_\eta \dot{\theta}^0(t) + \mathbf{V}_\eta \left[\left(\frac{1}{\eta^M} + \frac{1}{\eta^V}\right)\boldsymbol{\sigma}_\eta - \frac{E^V}{\eta^V \eta^V} \exp\left(-\frac{E^V t}{\eta^V}\right) \int_0^t \exp\left(\frac{E^V \tau}{\eta^V}\right) \boldsymbol{\sigma}_\eta(\tau)\, d\tau \right] \right\}, \tag{95}$$

where $\mathbf{V}_\eta$ is a (6×6) symmetric matrix with nonzero coefficients $V_{11} = V_{22} = V_{33} = 1$, $V_{44} = V_{55} = V_{66} = 2(1 + \nu_\eta)$, $V_{12} = V_{13} = V_{23} = -\nu_\eta$; where ν_η is the Poisson's ratio of Ω_η, assumed to be time-independent.

For the material constants required by the four-parameter model representing the ED-6 resin matrix, we adopt the values obtained by Wang and Weng (1992) from the creep data reported by Skudra and Auzukalns (1973): $E^M = 3.27$ GPa, $E^V = 1.8$ GPa, $\eta^M = 8000$ GPa.hr, $\eta^V = 300$ GPa.hr, $\nu = 0.38$. Elastic properties of the glass fiber were $E = 68.607$ GPa, $\nu = 0.21$.

In preparation for the solution of (95), the influence coefficients for the matrix $(\mathbf{F}_{\rho\eta}\mathbf{L}_\eta)$ were found using the computation procedure suggested by Eq. (83) for two different models of fibrous composites, the Mori-Tanaka model for two-phase materials, and the unit cell PHA model for the same two-phase material, with the subdivisions indicated in Figs. 4a (16 elements) and 4b (58 elements). For the two-phase materials, the $\mathbf{F}_{\rho\eta}$ factors are given by (22) in terms of the phase elastic compliance and stress concentration factors. The latter were evaluated with the Mori-Tanaka (1973) method, Benveniste (1987).

The solution itself was constructed both for step-constant and variable stress histories. In the first case, the overall creep compliances under axial tension σ_{11}, transverse tension σ_{22}, longitudinal shear σ_{12}, transverse shear σ_{23}, and transverse hydrostatic stress $\sigma_{22} = \sigma_{33}$ under plane strain ($\varepsilon_{11} = 0$) were computed from (95) with the solution algorithm described earlier. To avoid numerical difficulties, we replaced the overall step function by a ramp in which the overall stress was increased from 0.0 to 1.0 GPa in a small time interval equal 0.001 hr.

Individual overall creep compliances found from (95) for the two meshes in Figs. 4a, b ($M = 16$ and 58, respectively), and for the Mori-Tanaka approximation ($M = 2$) are shown in Figs. 10–14. Also shown in the figures are the results found from our reconstruction of the solution outlined by Wang and Weng (1992). These authors extended the Mori-Tanaka model to the Laplace domain, to examine the response of linearly viscoelastic materials under step loads. The Mori-Tanaka estimates of the overall moduli in the transformed domain were then inverted back into the real time domain to obtain the overall creep compliance functions. This inversion was carried out numerically using Legendre polynomials as suggested by Bellman et al. (1966).

As seen in Fig. 10, the overall response under axial straining is dominated by the elastic fiber. All creep compliance curves found with the various approximations considered above coincide in this case. On the other hand, the predicted overall creep compliances in normal and shear straining in the transverse plane, as well as in shear in the longitudinal plane, depend on the chosen model. The TFA solutions with 16 and 58 elements are similar. On the other hand, the approximation of the transformation concentration factors in the TFA method with Mori-Tanaka estimates of $\mathbf{B}_r$ in (22) provides lower magnitudes of the overall compliance, c.f., Figs. 11–14.

Viscoelastic response under sinusoidally changing load magnitudes was examined using again the above glass/ED-6 resin system. Solutions were obtained with the TFA method for the mesh shown in Fig. 4a (16 elements). The results appear in Figs. 15–18; they show the applied stress cycles and the variation of the corresponding coaxial strain components. The TFA method prediction suggests a nearly sinusoidal variation of the strains.

The procedure suggested by Wang and Weng (1992) was not applied to this sinusoidal loading since the numerical method they used for inverting the Laplace transform, in its original form, does not produce a sufficient number of points to represent the expected response. As Bellman et al. (1966) pointed out, this numerical procedure for computing the inversion of Laplace transform provides, with the proper change of time scale, approximate values for $\varepsilon(t)$ at the values $t_i = -\log x_i$, $i = 1, 2, \ldots, n$, where x_i are the n zeros of the shifted Legendre polynomial $P_n^*(x)$ which is defined for $0 \leqq x \leqq 1$. The roots of $P_n^*(x)$ are uniformly distributed to a higher degree of regularity as $n \to \infty$. However, $t_i = -\log x_i$ do not posses

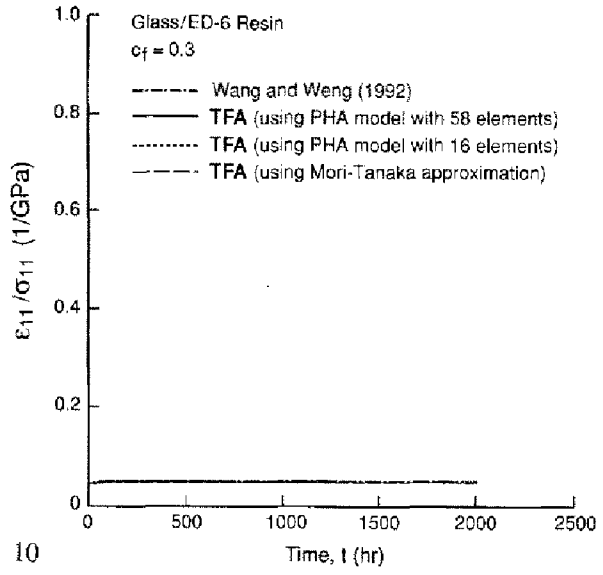

10

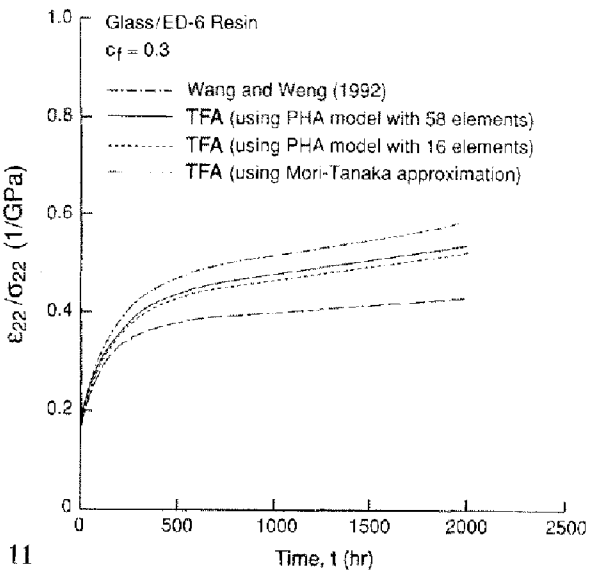

11

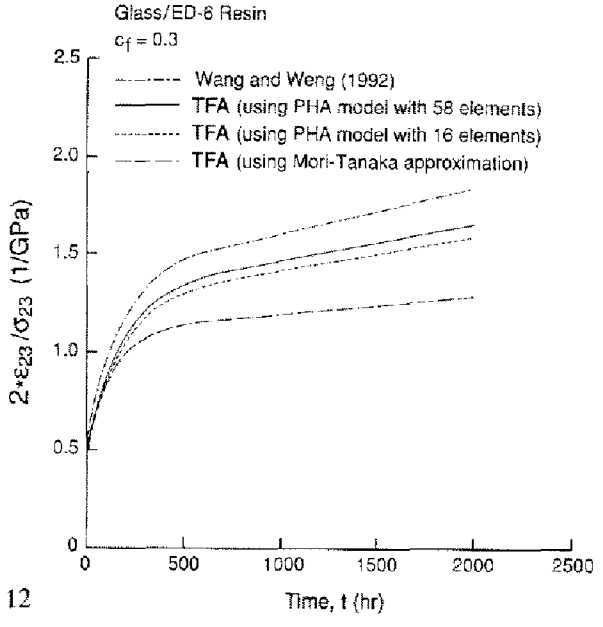

12

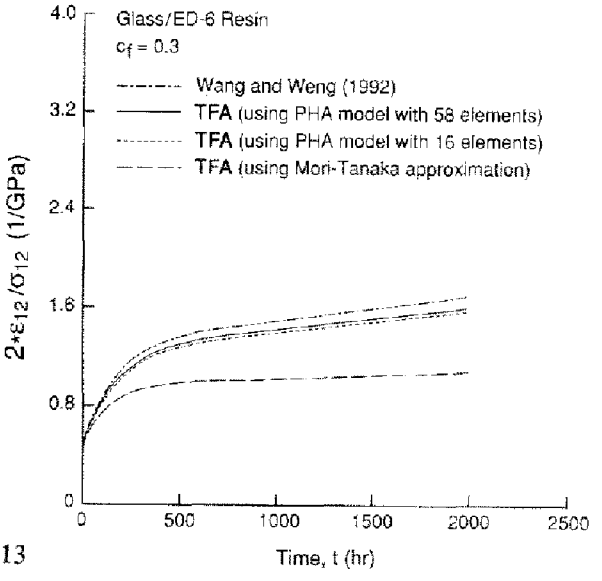

13

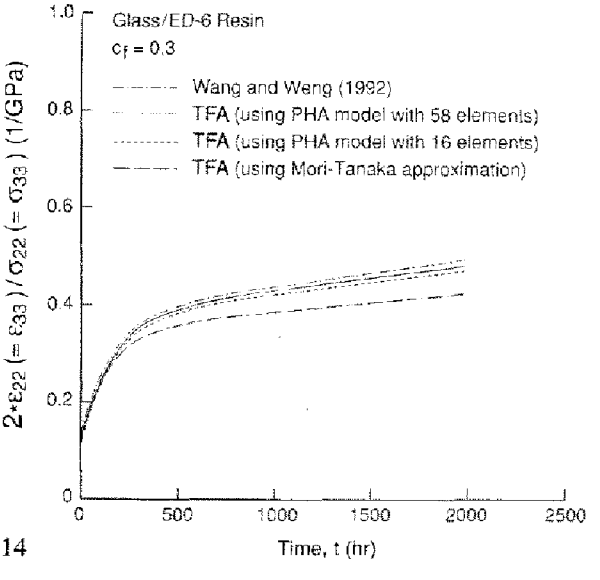

14

Figs. 10–14. 10 Creep compliance predictions for a glass/ED-6 resin composite subjected to axial tension. 11 Creep compliance predictions for a glass/ED-6 resin composite subjected to transverse tension. 12 Creep compliance predictions for a glass/ED-6 resin composite subjected to transverse shear. 13 Creep compliance predictions for a glass/ED-6 resin composite subjected to longitudinal shear. 14 Creep compliance predictions for a glass/ED-6 resin composite subjected to transverse isotropic tension under axial plane strain

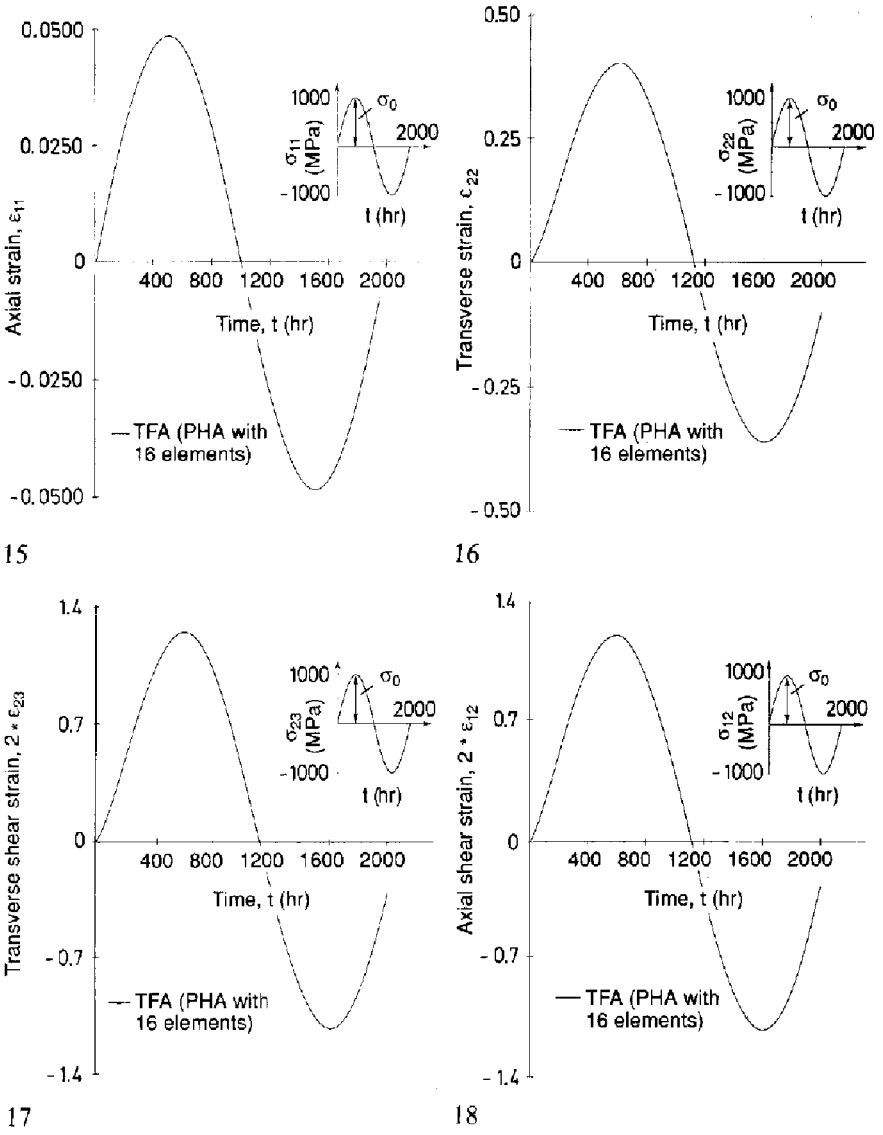

Figs. 15–18. 15 Strain predictions for a glass/ED-6 resin composite subjected to sinusoidal axial tensions. 16 Strain predictions for a glass/ED-6 resin composite subjected to sinusoidal transverse tension. 17 Strain predictions for a glass/ED-6 resin composite subjected to sinusoidal transverse shear. 18 Strain predictions for a glass/ED-6 resin composite subjected to sinusoidal longitudinal shear

the same equidistribution property over $0 \leqq t \leqq \infty$. In fact, the t_i values tend to congregate close to $t = 0$ and to scatter for large t. Increasing n, the order of $P_n^*(x)$, does not give significant improvement. Therefore, the response to sinusoidal loading is found only at irregularly spaced values of t.

In contrast, the TFA method can be applied for any selected resolution of the time scale. The method can also accommodate time-dependent multiaxial loads of changing magnitude and direction.

8
Viscoplastic systems

Another class of applications for the Eqs. (19), (20) or (60), (61) is found in heterogeneous media with viscoplastic phases. In this case, the local consititutive equations may be specified with a certain unified theory that connects the local inelastic strain rate $\dot{\boldsymbol{\varepsilon}}_\eta^{\text{in}}(t)$ to the local stress history, or the local relaxation stress rate $\dot{\boldsymbol{\sigma}}_\eta^{\text{re}}(t)$ to the local strain history. For example, the local inelastic strain rate may be specified by a power law of an internal stress variable R_η, as

$$\dot{\boldsymbol{\varepsilon}}_\eta^{\text{in}}(t) = \kappa_\eta(\theta) R_\eta^{p_\eta(\theta)} \mathbf{n}_\eta, \tag{96}$$

where $\kappa_\eta(\theta)$, $p_\eta(\theta)$ are material parameters for the element volume Ω_η, and $\mathbf{n}_\eta$ specifies the direction of the inelastic strain rate in the local stress space. When substituted into (20), with $\dot{\boldsymbol{\sigma}}_\eta^{\text{re}}(t) = -\mathbf{L}_\eta \dot{\boldsymbol{\varepsilon}}_\eta^{\text{in}}(t)$,

(96) provides the following differential equation for the local stresses,

$$\dot{\boldsymbol{\sigma}}_\rho(t) = \mathbf{B}_\rho \dot{\boldsymbol{\sigma}}^0(t) - \sum_{\eta=1}^{M} \mathbf{F}_{\rho\eta} \mathbf{L}_\eta \{ \mathbf{m}_\eta \dot{\theta}^0(t) + \kappa_\eta(\theta) R_\eta^{\bar{p}_\eta(\theta)} \mathbf{n}_\eta \}, \tag{97}$$

where $\boldsymbol{\sigma}^0(t)$ is the overall stress history and $\theta^0(t)$ is the temperature history. The power law (96) leads to a stiff differential equation (97) which requires integration by an implicit multistep method, such as the Adams method, with Newton iteration to solve the resulting nonlinear system of equations, and backward differentiation to evaluate the functional derivatives found in the Newton's method. Our solution of (97) utilized the IMSL fortran library version of the GEAR ordinary differential equation solver (Hindmarsh 1974) which implements the solution procedure developed by Gear (1971) for stiff differential equations.

To illustrate this procedure, we examined the time-dependent response of a SCS6/Ti-15-3 fibrous composite with 30% fiber volume concentration at 482 °C. At this temperature, the fiber is assumed to be elastic with $E = 397.8$ GPa and $\nu = 0.25$. The titanium matrix is assumed to be elastic-viscoplastic. A specific form of (96) was obtained from the viscoplasticity theory of Eisenberg and Yen (1981). In this case, the internal variable R is an invariant of the overstress tensor $(\boldsymbol{\sigma} - \boldsymbol{\sigma}^*)$, where $\boldsymbol{\sigma}$ is the current stress and $\boldsymbol{\sigma}^*$ is the equilibrium, quasi-static stress. The latter is defined by an equilibrium yield surface. Evolution of the equilibrium yield surface and the overstress was specified with the constitutive equations derived by Bahei-El-Din et al. (1991) and Shah (1991). These equations allow for both kinematic and isotropic hardening of the yield surface under inelastic straining, and for thermal recovery. They also employ a two-surface plasticity theory to define the quasi-static response. A summary of the relevant constitutive equations is given in Appendix C. The material parameters for a titanium matrix at 482 °C were found from the data given by Johnson et al. (1993) and are given here in Table 7.

The PHA model, with the unit cell subdivision of Fig. 4a was used in derivation of the mechanical and eigenstress concentration factors $\mathbf{B}_\rho$ and $\mathbf{F}_{\rho\eta}$. Then, Eqs. (96), (97) and the evolution equations given in Appendix C were integrated for loading at the constant uniaxial transverse tension stress $\sigma_{22} = 500$ MPa, reached at two time rates, 0.5 MPa/sec and 5.0 MPa/sec. The integration was performed using the GEAR solver with a tolerance of 0.001. Figures 19 and 20 show the stress-strain response and the

Table 7. Elastic-thermo-viscoplastic constants of T_i-15-3 matrix at 482 °C

Material constant[‡]	Units	Value
E	GPa	72.2
ν		0.351
Y	MPa	142.0
$\mathscr{Y}$	MPa	223.0
H_0	MPa	83.0
h	GPa	1.6
p		5.68
k	$(\text{MPa})^{-p}$/sec	4.53×10^{-19}

[‡] Script letters are related to the bounding surface, Appendix C

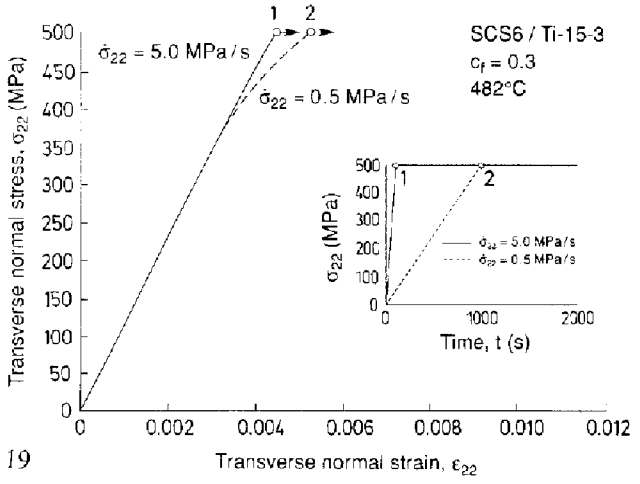

19

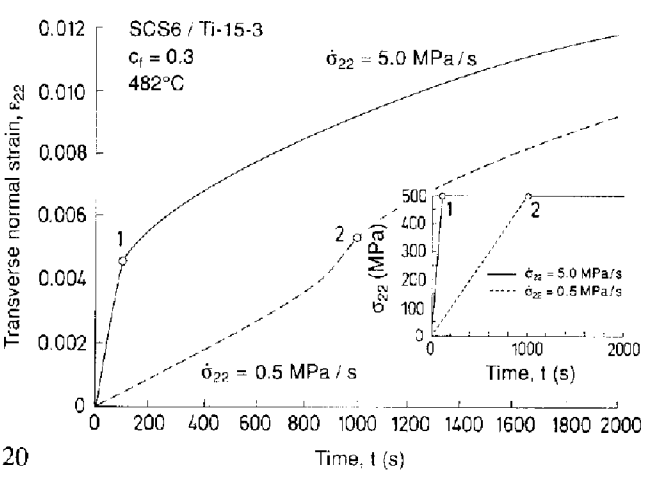

20

Figs. 19–20. 19 Transverse normal stress-strain response computed with the TFA method for a viscoplastic SCS6/Ti-15-3 composite. 20 Transverse normal strain-time response computed with the TFA method for a viscoplastic SCS6/Ti-15-3 composite

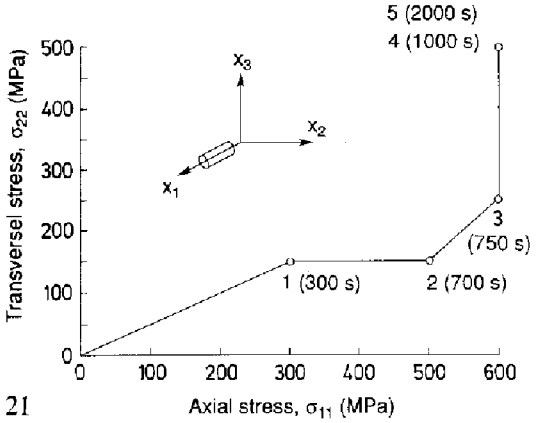

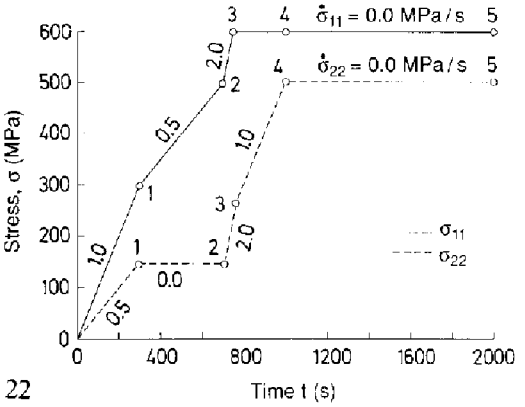

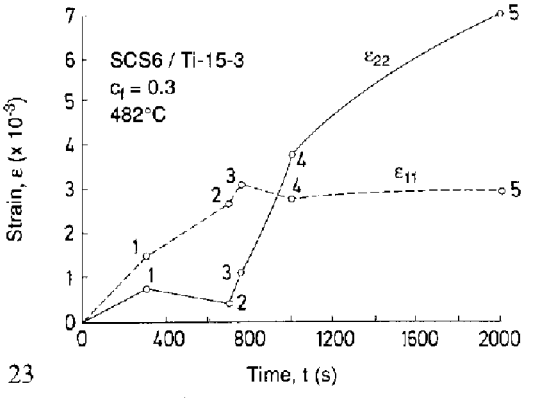

Figs. 21–23. 21 Axial tension-transverse tension path applied to the viscoplastic SCS6/Ti-15-3 composite. 22 Time history of axial and transverse stresses for the loading path of Fig. 21. 23 Overall stress-strain histories predicted by the TFA method for the loading path of Figs. 21 and 22

strain-time history computed with the TFA method. No other solutions appear to be available for comparison.

Another example was constructed with the TFA method for the biaxial stress path shown in Figs. 21 and 22. The corresponding overall strain is shown in Fig. 23, together with the creep strains computed in the time segment 4–5, Fig. 22.

9
Conclusions

The transformation field analysis is a general method for solving inelastic deformation and other incremental problems in heterogeneous media with many interacting inhomogeneities. The various unit cell models, or the corrected inelastic self-consistent or Mori-Tanaka fomulations, the so-called Eshelby method, and the Eshelby tensor itself are all seen as special cases of this more general approach. The method easily accommodates any uniform overall loading path, inelastic constitutive equation and micromechanical model. The model geometries are incorporated through the mechanical transformation influence functions or concentration factor tensors which are derived from elastic solutions for the chosen model and phase elastic moduli. Thus, there is no need to solve inelastic boundary value or inclusion problems, indeed such solutions are typically associated with erroneous procedures that violate (6_2); this was discussed by Dvorak (1992). In comparison with the finite element method in unit cell model solutions, the present method is more efficient for cruder meshes. Moreover, there is no need to implement inelastic constitutive equations into a finite element program. An addition to the examples shown herein, the method can be applied to many other problems, such as those arising in active materials with eigenstrains induced by components made of shape memory alloys or other actuators. Progress has also been made in applications to electroelastic composites, and to problems involving damage development in multiphase solids. Finally, there is no conceptual obstacle to extending the approach beyond the analysis of representative volumes of composite materials, to arbitrarily loaded structures.

Appendix A

This is a brief summary of constitutive equations for elastic-plastic homogeneous materials subjected to uniform stress or strain and temperature changes. Response under such thermomechanical loads is determined with the help of a yield surface $g(\boldsymbol{\sigma}, \theta) = 0$ which contains the stress states that cause purely elastic deformations. Assuming kinematic and isotropic hardening, the Mises form of the yield surface

is given by

$$g(\boldsymbol{\sigma},\theta) \equiv \frac{3}{2}(\mathbf{s}-\mathbf{a}):(\mathbf{s}-\mathbf{a}) - Y^2(\theta) = 0, \tag{A-1}$$

where s is the deviatoric stress, a is the center of the yield surface in the deviatoric stress space, Y is the yield stress in simple tension. In (A-1), we used the notation (a:b) to denote the inner product of second order tensors a_{ij} and b_{ij}. The elastic behavior is in effect if $g < 0$, or if $g = 0$ and $[(\partial g/\partial \boldsymbol{\sigma}):d\boldsymbol{\sigma} + (\partial g/\partial\theta)\,d\theta] \leqq 0$. On the other hand, elastic-plastic deformation takes place if $g = 0$ and $[(\partial g/\partial \boldsymbol{\sigma})\,d\boldsymbol{\sigma} + (\partial g/\partial\theta)\,d\theta] > 0$. In this case, the instantaneous plastic compliance $\mathscr{M}^P$, stiffness $\mathscr{L}^P$, and the thermal strain and stress vectors $\mathscr{m}^P$, $\mathscr{\ell}^P$ in (64) are given by (Bahei-El-Din 1990; Shah 1991)

$$\mathscr{M}^P = (3/2H)(\mathbf{n}:\mathbf{n}^T) \quad \mathscr{L}^P = -(2G/(1+H/3G))(\mathbf{n}:\mathbf{n}^T) \tag{A-2}$$

$$\mathscr{m}^P = -((\sqrt{3}\,Y'(\theta))/(\sqrt{2}H))\,\mathbf{n} \tag{A-3}$$

$$\mathscr{\ell}^P = (2G/(1+H/3G))(\mathbf{n}^T\mathbf{m} + (Y'(\theta)/\sqrt{6}G))\,\mathbf{n} \tag{A-4}$$

$$H = (d\bar{\sigma} - Y'(\theta)\,d\theta)/d\bar{\varepsilon}^P, \quad d\bar{\sigma} = \sqrt{\left(\frac{3}{2}d\mathbf{s}:d\mathbf{s}\right)}, \quad d\bar{\varepsilon}^P = \sqrt{\left(\frac{2}{3}d\boldsymbol{\varepsilon}^P:d\boldsymbol{\varepsilon}^P\right)} \tag{A-5}$$

$$\mathbf{n} = (1/\sqrt{(2/3)}\,Y)\,[\bar{s}_{11}\,\bar{s}_{22}\,\bar{s}_{33}\,2\bar{s}_{32}\,2\bar{s}_{31}\,2\bar{s}_{12}]^T, \quad \bar{\mathbf{s}} = \boldsymbol{\sigma} - \mathbf{a}. \tag{A-6}$$

Here, G is the elastic shear modulus, $Y'(\theta) = dY/d\theta$, $\boldsymbol{\varepsilon}^P$ is the plastic strain vector, and H is plastic tangent modulus of the stress-plastic strain curve. The product $\mathbf{n}:\mathbf{n}^T$ in (A-2) denotes the tensor product $n_{ij}n_{kl}$; $\mathbf{m}$ is the elastic thermal strain tensor.

Evolution of the center of the matrix yield surface a and the plastic tangent modulus H may be described in several different ways, to fit experimental observations. Specific forms of the Prager-Ziegler and Phillips hardening rules for thermomechanical loads can be found in (Bahei-El-Din 1990; Dvorak 1991; Shah 1991). Variation of the plastic tangent modulus H can be found with a two surface plasticity theory such as the theory given by Dafalias and Popov (1976).

Appendix B

Here we give expression for the creep compliance tensor $\mathbf{J}(t)$ of the four-parameter model consisting of the Maxwell and Voigt elements in series. Let the E^M, η^M, E^V, and η^V, denote the linear spring constant and the coefficient of viscosity for the Maxwell and Voigt models, repectively. The longitudinal creep compliance function for the four-parameter solid is given by (Findley 1976)

$$J_A(t) = \frac{1}{E^M} + \frac{1}{E^V}\left[1 - \exp\left(-\frac{E^V t}{\eta^V}\right)\right] + \frac{t}{\eta^M}. \tag{B-1}$$

Assuming that the Poisson's ratio ν of the material is not a function of time, then the transverse creep compliance is a function only of the longitudinal creep compliance (Christensen 1971; Sternstein 1977; Sternstein and Ho 1972):

$$J_T(t) = -\nu J_A(t). \tag{B-2}$$

The shear and longitudinal creep compliances are also related by

$$J_S(t) = 2(1+\nu)J_A(t). \tag{B-3}$$

These relations are assumed to represent uniaxial response of an isotropic homogeneous solid. A more general form of the creep compliance in three dimensions can be written in the form

$$\mathbf{J}(t) = J_A(t)\,\mathbf{V}, \quad \mathbf{V} = \begin{bmatrix} 1 & -\nu & -\nu & 0 & 0 & 0 \\ & 1 & -\nu & 0 & 0 & 0 \\ & & 1 & 0 & 0 & 0 \\ & & & 2(1+\nu) & 0 & 0 \\ & & & & 2(1+\nu) & 0 \\ \text{sym.} & & & & & 2(1+\nu) \end{bmatrix} \tag{B-4}$$

Differentiating (B-4) with respect to time, we find

$$\dot{\mathrm{J}}(t) = \dot{J}_A(t)\,\mathrm{V} = \left[\frac{1}{\eta^M} + \frac{1}{\eta^V}\exp\left(-\frac{E^V t}{\eta^V}\right)\right]\mathrm{V} \tag{B-5}$$

$$\ddot{\mathrm{J}}(t) = \ddot{J}_A(t)\,\mathrm{V} = \left[-\frac{E^V}{\eta^V\eta^V}\exp\left(-\frac{E^V t}{\eta^V}\right)\right]\mathrm{V}. \tag{B-6}$$

Then,

$$\dot{\mathrm{J}}(0) = \left(\frac{1}{\eta^M} + \frac{1}{\eta^V}\right)\mathrm{V}, \tag{B-7}$$

$$\ddot{\mathrm{J}}(t-\tau) = \left[-\frac{E^V}{\eta^V\eta^V}\exp\left(-\frac{E^V t}{\eta^V}\right)\exp\left(\frac{E^V \tau}{\eta^V}\right)\right]\mathrm{V}. \tag{B-8}$$

Appendix C

Here we summarize the constitutive equations of the unified viscoplastic response given by (Bahei-El-Din et al. 1991; and Shah 1991). As indicated by (3_1), the total strain rate is decomposed into elastic, thermal and inelastic parts. The inelastic strain is found as a function of the overstress measured from an equilibrium yield surface which contains all stress states that can be reached from the current state by purely elastic deformation. A Mises form of the equilibrium surface is written as

$$g = \frac{3}{2}(s_{ij}^* - a_{ij})(s_{ij}^* - a_{ij}) - (Y+Q)^2 = 0, \tag{C-1}$$

where s_{ij}^* is the deviatoric equilibrium stress tensor, a_{ij} denotes the center of the yield surface, $Y = Y(\theta)$ is the initial yield stress in tension, and is independent of the loading rate, and $Q = Q(\theta)$ is an isotropic hardening function.

For a given stress tensor s_{ij}, which lies outside the yield surface (C-1), there exists an equilibrium stress s_{ij}^* which satisfies (C-1) such that

$$s_{ij}^* = \left[\frac{2[Y+Q]^2}{3(s_{k_\ell} - a_{k_\ell})(s_{k_\ell} - a_{k_\ell})}\right]^{1/2}(s_{ij} - a_{ij}) + a_{ij}. \tag{C-2}$$

The effective overstress R is a measure of the distance between the actual stress point s_{ij} and the equilibrium stress point s_{ij}^*. It vanishes if the stress point lies on, or falls inside the yield surface. In particular,

$$R = \left[\frac{3}{2}(s_{ij} - s_{ij}^*)(s_{ij} - s_{ij}^*)\right]^{1/2} \quad \text{if } g(s_{ij} - a_{ij}) > 0, \tag{C-3}$$

$$R = 0 \qquad \text{if } g(s_{ij} - a_{ij}) \leqq 0. \tag{C-4}$$

The inelastic strain rate is then written as

$$\dot{\varepsilon}_{ij}^{\mathrm{in}} = \sqrt{(3/2)}\,k(\theta)\,R^{p(\theta)}\,n_{ij}, \tag{C-5}$$

where the functions $k(\theta)$ and $p(\theta)$ are material parameters and n_{ij} is a unit normal to the yield surface (C-1) at the current equilibrium stress point. From (C-1) one finds this as

$$n_{ij} = \frac{(s_{ij}^* - a_{ij})}{[(s_{k_\ell}^* - a_{k_\ell})(s_{k_\ell}^* - a_{k_\ell})]^{1/2}} = \sqrt{(3/2)}\,\frac{(s_{ij}^* - a_{ij})}{(Y+Q)}. \tag{C-9}$$

The evolution equation for Q which includes the effect of inelastic deformation and thermal recovery on the yield stress is given by

$$\dot{Q} = q(\theta)[Q_a(\theta) - Q]\,\dot{\varepsilon}^{\mathrm{in}} - b_r(\theta)|Q - Q_r(\theta)|^{(n_r(\theta)-1)}[Q - Q_r(\theta)]. \tag{C-7}$$

The functions $q(\theta)$, $Q_a(\theta)$, $b_r(\theta)$, $Q_r(\theta)$, and $n_r(\theta)$ are material parameters, and $\dot{\bar{\varepsilon}}^{in}$ is the effective inelastic strain rate;

$$\dot{\bar{\varepsilon}}^{in} = \left[\frac{2}{3}\dot{\varepsilon}^{in}_{ij}\dot{\varepsilon}^{in}_{ij}\right]^{1/2} = k(\theta)R^{p(\theta)}; \quad \dot{\varepsilon}^{in}_{kk} = 0. \tag{C-8}$$

Total ($Q_r = 0$), or partial ($Q_r \neq 0$) thermal recovery is represented by the second term in (C-7).

In analogy with (C-7), and permitting complete thermal recovery of kinematic hardening, the evolution equation for the center of the yield surface a_{ij} can be written as

$$\dot{a}_{ij} = \dot{\mu}\, v_{ij} - v_r(\theta)\bar{a}^{(w_r(\theta)-1)}a_{ij}, \quad \bar{a} = (a_{k_r}a_{k_r})^{1/2} \tag{C-9}$$

where $v_r(\theta)$ and $w_r(\theta)$ are material parameters. The unit tensor v_{ij} defines the direction of translation of the yield surface in the deviatoric stress space, and can be specified according to the hardening rules applied in rate-independent plasticity theories. If the Phillips hardening rule is selected, then

$$v_{ij} = \dot{s}_{ij}/(\dot{s}_{k_e}\dot{s}_{k_e})^{1/2} \quad \text{if } \dot{s}_{ij} \neq 0 \tag{C-10}$$

$$v_{ij} = n_{ij} \quad \text{if } \dot{s}_{ij} = 0. \tag{C-11}$$

The factor $\dot{\mu}$ in (C-9) is found from Prager's consistency condition $\dot{g} = 0$, when translation of the yield surface is specified by the first term in (C-9). The result is

$$\dot{\mu} = \sqrt{(2/3)}\,k(\theta)R^{p(\theta)}[H(\theta) - q(\theta)[Q_a(\theta) - Q]]/n_{k_i}v_{k_i}. \tag{C-12}$$

A two-surface plasticity theory (Dafalias and Popov, 1976) can be used to describe evolution of the instantaneous tangent modulus H:

$$H(\theta) = H_0(\theta) + h(\theta)[\delta/(\delta_0 - \delta)], \tag{C-13}$$

$$\delta = \left[\frac{3}{2}(\bar{s}_{ij} - s^*_{ij})(\bar{s}_{ij} - s^*_{ij})\right]^{1/2}, \tag{C-14}$$

where δ_0 is the distance between the yield surface and the bounding surface at the onset of inelastic deformation. Here, $\bar{s}_{ij}$ is the deviatoric bounding stress tensor determined from equality of the normal to the equilibrium yield surface $n_{ij}(s^*_{ij})$, Eq. C-6, and the normal to the bounding surface $\bar{n}_{ij}(\bar{s}_{ij})$. When the equilibrium stress point lies on the bounding surface, the plastic tangent modulus $H(\theta)$ assumes the asymptotic value $H_0(\theta)$, which together with the parameter $h(\theta)$ need to be determined experimentally. In analogy with the equilibirum yield surface, thermal recovery of isotropic as well as kinematic hardening of the bounding surface can be included in the model. This is omitted here for brevity. We only mention that the recovery terms for isotropic and kinematic hardening of the bounding surface assume a form similar to those suggested above for the yield surface, but with new material parameters.

The material parameters of the Ti-15-3 alloy, required by the present theory, were found from the data given by Johnson et al. (1993). Table 7 shows the parameters at 482 °C, where the script Latin letters refer to the bounding surface but have the same interpretation as their yield surface counterparts. For example, the Mises form of the bounding surface is written as

$$\mathscr{g} = \frac{3}{2}(\bar{s}_{ij} - \mathscr{a}_{ij})(\bar{s}_{ij} - \mathscr{a}_{ij}) - (\mathscr{y} + \mathscr{Q})^2 = 0, \tag{C-15}$$

where $\mathscr{a}_{ij}$ is the center of the bounding surface, $\mathscr{y} = \mathscr{y}(\theta)$ is the bounding stress given by the intersection of the asymptotic part of the uniaxial stress-plastic strain curve and the stress axis, and $\mathscr{Q} = \mathscr{Q}(\theta)$ is an isotropic hardening function. Material parameters not shown in Table 7 assumed to be equal to zero.

References

Bahei-El-Din, Y. A. 1990: Plasticity analysis of fibrous composite laminates under thermomechanical loads. In: Kennedy, J. M.; Moeller, H. H.; Johnson, W. S. (ed.): Thermal and mechanical behavior of metal matrix and ceramic matrix composites. ASTM STP 1080: 20–39. American Society for Testing and Materials, Philadelphia, PA

Bahei-El-Din, Y. A.; Shah, R. S.; Dvorak, G. J. 1991: Numerical analysis of the rate-dependent behavior of high temperature fibrous composites. In: Singhal, S. N.; Jones, W. F.; Cruse, T.; Herakovich, C. T. (ed.): Mechanics of composites at elevated and cryogenic temperatures. ASME AMD 188: 67–78. American Society of Mechanical Engineers, New York, NY

Bellman, R. E.; Kalaba, R. E.; Lockett, J. A. 1966: Numerical inversion of the Laplace transform. Elsevier, New York
Benveniste, Y. 1987: A new approach to the application of Mori-Tanaka's theory in composite materials. Mech. of Materials 6: 147–157
Christensen, R. M. 1971: Theory of viscoelasticity, an introduction. Academic Press, New York
Christersen, R. M. 1979: Mechanics of composite materials. John Wiley, New York
Dafalias, Y. F.; Popov, E. P. 1976: Plastic internal variables formalism of cyclic plasticity. J. Appl. Mech. 43: 645–651
Dvorak, G. J. 1990: On uniform fields in heterogeneous media. Proc. R. Soc. Lond. A 431: 89–110
Dvorak, G. J. 1991: Plasticity theories for fibrous composite materials. In: Everett, R. K.; Arsenault, R. J. (ed.): Metal matrix composites, Mechanisms and properties, vol. 2: 1–77. Academic Press, Boston
Dvorak, G. J. 1992: Transformation field analysis of inelastic composite materials. Proc. R. Soc. Lond. A 437: 311–327
Dvorak, G. J.; Benveniste, Y. 1992: On transformation strains and uniform fields in multiphase elastic media. Proc. R. Soc. Lond. A 437: 291–310
Dvorak, G. J.; Teply, J. L. 1985: Periodic hexagonal array models for plasticity analysis of composite materials. In: Sawczuk, A.; Bianchi, V. (ed.): Plasticity today: Modeling, methods and applications, W. Olszak memorial volume, 623–642. Elsevier Science Publishers, Amsterdam
Eisenberg, M. A.; Yen, C. F. 1981: A theory of multiaxial anisotropic viscoplasticity. J. Appl. Mech. 48: 276–284
Findley, W. N.; Lai, J. S.; Onaran, K. 1976: Creep and relaxation of nonlinear viscoelastic materials. North-Holland Publishing Co., Amsterdam
Gear, C. W. 1971: Numerical initial value problems in ordinary differential equations. Prentice-Hall, Englewood Cliffs, New Jersey
Hill, R. 1963: Elastic properties of reinforced solids: Some theoretical principles. J. Mech. Phys. Solids. 11: 357–372
Hindmarsh, A. C. 1974: GEAR: Ordinary differential equations system solver. Lawrence Livermore Laboratory, Report UCID-30001, Revision 3.
Johnson, W. S.; Mirdamadi, M.; Bahei-El-Din, Y. A. 1993: Stress-strain analysis of a $[0/90]_{2s}$ titanium matrix laminate subjected to a generic hypersonic flight profile. J. Composites Technology and Research, 15: 297—303.
Laws, N. 1973: On the thermostatics of composite materials. J. Mech. Phys. Solids. 21: 9–17
Levin, V. M. 1967: Thermal expansion coefficients of heterogeneous materials. Mekhanika Tverdogo Tela. 2: 88–94, English Translation: Mech. of Solids. 11: 58–61
Mori, T.; Tanaka, K. 1973: Average stress in matrix and average elastic energy of materials with misfitting inclusion. Acta Metal. 21: 571–574
Shah. R. S. 1991: Modeling and analysis of high temperature inelastic deformation in metal matrix composites. Ph.D. Thesis, Rensselaer Polytechnic Institute, Troy, New York
Skudra, A. M.; Auzukalns, Y. V. 1973: Creep and long-term strength of unidirectional reinforced plastics in compression. Polymer Mech. 6: 718–722
Sloan, S. W. 1987: Substepping schemes for the numerical integration of elastoplastic stress-strain relations. Int. J. Num. Meth. Engng. 24: 893–911
Sternstein, S. S. 1977: Mechanical properties of glassy polymers. In: Herman, H. (ed.): Treatise on Materials Science and Technology, vol. 10: part B 541–598. Academic Press, New York
Sternstein, S. S.; Ho, T. C. 1972: Biaxial stress relaxation in glassy polymers: Polymethyl metchacrylate. J. Appl. Phys. 43: 4370–4383
Teply, J. L.; Dvorak, G. J. 1988: Bounds on overall instantaneous properties of elastic-plastic composites. J. Mech. Phys. Solids 36: 29–58
Wang, Y. M.; Weng, G. J. 1992: The influence of inclusion shape on the overall viscoelastic behavior of composites. J. Appl. Mech. 59: 510–518